Naval Environmental Prediction Research Facility
Monterey, CA 93943-5006
Technical Report TR 88-02 February 1988

AN EVALUATION OF TWO MILLIMETER WAVE PROPAGATION MODELS FOR HORIZONTAL ATMOSPHERIC ATTENUATION AT 70-115 GHZ

Gerard N. Vogel
Naval Environmental Prediction Research Facility

REPORT DOCUMENTATION PAGE

1a. REPORT SECURITY CLASSIFICATION UNCLASSIFIED	1b. RESTRICTIVE MARKINGS
2a. SECURITY CLASSIFICATION AUTHORITY	3. DISTRIBUTION/AVAILABILITY OF REPORT Approved for public release; distribution unlimited
2b. DECLASSIFICATION/DOWNGRADING SCHEDULE	
4. PERFORMING ORGANIZATION REPORT NUMBER(S) TR 88-02	5. MONITORING ORGANIZATION REPORT NUMBER(S)
6a. NAME OF PERFORMING ORGANIZATION Naval Environmental Prediction Research Facility 6b. OFFICE SYMBOL (If applicable)	7a. NAME OF MONITORING ORGANIZATION
6c. ADDRESS (City, State, and ZIP Code) Monterey, CA 93943-5006	7b. ADDRESS (City, State, and ZIP Code)
8a. NAME OF FUNDING/SPONSORING ORGANIZATION EM Propagation Div. Naval Ocean Systems Center 8b. OFFICE SYMBOL (If applicable) Code 54	9. PROCUREMENT INSTRUMENT IDENTIFICATION NUMBER
8c. ADDRESS (City, State, and ZIP Code) San Diego, CA 92152	10. SOURCE OF FUNDING NUMBERS PROGRAM ELEMENT NO. 62435N; PROJECT NO. RA35G80; TASK NO.; WORK UNIT ACCESSION NO. DN656761

11. TITLE (Include Security Classification)
An Evaluation of Two Millimeter Wave Propagation Models for Horizontal Atmospheric Attenuation at 70-115 GHz (U)

12. PERSONAL AUTHOR(S) Vogel, Gerard N.

13a. TYPE OF REPORT	13b. TIME COVERED	14. DATE OF REPORT (Year, Month, Day)	15. PAGE COUNT
Final	FROM 5/87 TO 8/87	1988, February	82

16. SUPPLEMENTARY NOTATION

17. COSATI CODES			18. SUBJECT TERMS (Continue on reverse if necessary and identify by block number)
FIELD	GROUP	SUB-GROUP	Atmospheric attenuation Millimeter wave Propagation model
04	01		
04	02		

19. ABSTRACT (Continue on reverse if necessary and identify by block number)
An evaluation is performed for two millimeter wave propagation models: the LIEBE model, developed at the Institute for Telecommunications, Boulder, CO, under the guidance of Dr. H. Liebe; and the EOSAEL model, developed at the US Army Atmospheric Laboratory at White Sands Missile Range, NM. This evaluation is conducted for horizontal attenuation due to both clear atmosphere and hydrometeor effects under typical surface meteorological conditions, and within the frequency range 70-115 GHz. Intercomparisons of model theories and predictions show slight differences for molecular oxygen and fog attenuations, but significant differences for water vapor and rain attenuations. Results indicate that, while the qualitative agreement between either the EOSAEL or LIEBE model predictions, and measurements, for horizontal attenuation due to oxygen, water vapor, fog and rain is certainly satisfactory, there is a definite need for improvement. Overall, no clear preference for either the EOSAEL or LIEBE model for operational use is ascertained. Data comparisons suggest that, for several attenuation types, model preference is dependent on either the frequency or meteorological conditions.

20. DISTRIBUTION/AVAILABILITY OF ABSTRACT ☒ UNCLASSIFIED/UNLIMITED ☐ SAME AS RPT. ☐ DTIC USERS	21. ABSTRACT SECURITY CLASSIFICATION UNCLASSIFIED
22a. NAME OF RESPONSIBLE INDIVIDUAL Vogel, Gerard N.	22b. TELEPHONE (Include Area Code) (408) 647-4766 22c. OFFICE SYMBOL NEPRF WU 6.2-11

DD FORM 1473, 84 MAR 83 APR edition may be used until exhausted. All other editions are obsolete.

TABLE OF CONTENTS

1. INTRODUCTION

Recent advancements in millimeter wave technology have spurred the development of millimeter wave propagation models capable of realistically incorporating atmospheric effects on predictions of system performance. Two such models, the LIEBE model, developed at the Institute for Telecommunications in Boulder, CO., under the guidance of Dr. H. Liebe, and the EOSAEL model, developed at the U.S. Army Atmospheric Sciences Laboratory at White Sands Missile Range, NM, are evaluated in this report.

This evaluation is conducted for horizontal attenuation of millimeter waves due to molecular oxygen, water vapor, fog, and rain under typical surface meteorological conditions, and within the frequency range 70-115 GHz. First, in section two, the theoretical bases of the LIEBE and EOSAEL models are compared, along with model predictions for typical surface meteorological conditions. Then, in section three, a systematic comparison is made between the LIEBE and EOSAEL model predictions of attenuation and available measurements which could be located in the literature.

2. COMPARISON OF MODELS

2.1 General Considerations

The LIEBE millimeter wave propagation model is both more complex and larger than the EOSAEL model, due in large part to two features not found in the EOSAEL model: first, the capability to calculate zenith attenuation and refractive dispersion; and second, a capability for the calculation of isolated line

behavior (especially Zeeman patterns of O_2 lines) in the mesosphere. On the other hand, the less complex EOSAEL model contains several features not found in the LIEBE model: the calculation of attenuation due to snow, and the calculation of backscatter cross sections for fog, rain and snow. Notwithstanding, it is the many similarities in model formulation and structure which makes a comparison of the LIEBE and EOSAEL millimeter wave propagation models feasible.

In this section, the LIEBE and EOSAEL model formulations and predictions of horizontal atmospheric attenuation due to clear air and hydrometeor effects are examined and compared. These model comparisons are made for typical surface meteorological conditions over the frequency range of 70-115 GHz (see Table 2-1).

The meteorological parameters required as input by the LIEBE and EOSAEL models in the calculation of oxygen, water vapor, gaseous (oxygen plus water vapor), liquid water and rain attenuations are shown in Table 2-1. It is observed that the EOSAEL model permits as input either the relative or absolute humidity for gaseous attenuation predictions. Unlike the LIEBE model, the EOSAEL model requires a temperature input for the calculation of rain attenuation, as well as permits a specification of rain type. Since the EOSAEL model computes the transmission as well as the specific attenuation, an input value of 1 km is specified for the path length for all computer runs.

Table 2-1. Input Meteorological Parameters Required (and values assigned) in the Calculations of Oxygen, Water Vapor, Gaseous, Liquid Water and Rain Attenuations by the EOSAEL(E) and LIEBE(L) Models.

INPUT		ATTENUATION									
		OXYGEN		WATER VAPOR		GASEOUS		LIQUID WATER		RAIN	
Parameter	Value(s)	E	L	E	L	E	L	E	L	E	L
Frequency	70-115 GHz	X	X	X	X	X	X	X	X	X	X
Temperature	0-30°C	X	X	X	X	X	X	X	X	X	
Pressure	1 atm	X	X	X	X	X	X				
Relative Humidity	0-100%	X	X	X	X	X	X				
Absolute Humidity	0-20 g/m^3	X		X		X					
Liquid Water Content	0-1 g/m^3							X	X		
Rain Rate	0.2-100 mm/hr									X	X
Rain Type										X	

For this study, attenuation predictions by the LIEBE and EOSAEL models were performed on an HP9020 minicomputer - the LIEBE model without the zenith attenuation and mesosphere subprograms. With a comparable and relatively modest number of lines of FORTRAN code (several hundred), computer run times of both models were very fast for individual predictive calculations.

2.2 Clear Atmosphere Effects

2.2.1 Oxygen Absorption

The frequency range chosen for this study (70-115 GHz) is a transmission window between a molecular oxygen (O_2) absorption line complex centered near 60 GHz and a single O_2 absorption line at 118.75 GHz.

The procedures employed by the LIEBE and EOSAEL models in the calculation of molecular oxygen absorption are very similar; in fact, the EOSAEL model is based on the theory and experimental results given by Liebe et al. (1977). The LIEBE model defines oxygen absorption (in db/km) as

$$\alpha_{O_2}(f) = .182f \left[\sum_{i=1}^{n} (S_i F_i) + N_p \right] \qquad (1)$$

where f is the frequency (GHz), n is the number of oxygen resonance lines, S_i is the strength of the ith line, F_i is the line shape factor (line profile) for the ith line and N_p is a dry air continuum spectra due to nonresonant O_2 and pressure induced N_2 absorption. The terms S_iF_i and N_p are given in ppm. This formulation, less the term N_p, is used in the EOSAEL model.

The number of oxygen resonance lines is 42 for the EOSAEL model and 48 for the LIEBE model. Both models employ essentially the same 41 lines for the 60 GHz complex as well as one line at 118.75 GHz, with the LIEBE model using six additional lines at higher frequencies. Interestingly, for p = 1 atm., T=[0,30]°C and f=[70,115] GHz, the LIEBE model predicts the same oxygen absorption with or without the additional six O_2 resonance lines.

Both models utilize the modified Van Vleck-Weisskopf form for each absorption line profile, given as

$$F(f, f_o, \gamma, \delta) = \frac{f}{f_o}\left[\frac{\gamma - (f_o - f)\,\delta}{(f_o - f)^2 + \gamma^2} + \frac{\gamma - (f_o + f)\,\delta}{(f_o + f)^2 + \gamma^2}\right] \qquad (2)$$

where f_o is the line center frequency, γ is the line halfwidth and δ is a pressure and temperature dependent line overlap correction. The line strength S_i and the line parameters γ and δ are calculated by means of pressure and temperature dependent empirical formulae in the LIEBE model and are given as data tables in the EOSAEL model. The dry air continuum N_p, also calculated empirically, is defined in Liebe (1985a,b).

Oxygen absorption at several temperatures, as predicted by the LIEBE model, is displayed in Figure 2-1. A minimum is noted near 100 GHz, with sharply higher values of O_2 absorption at the window wings. The absorption is inversely proportional to temperature at all frequencies. These characteristics also apply to the EOSAEL model predictions.

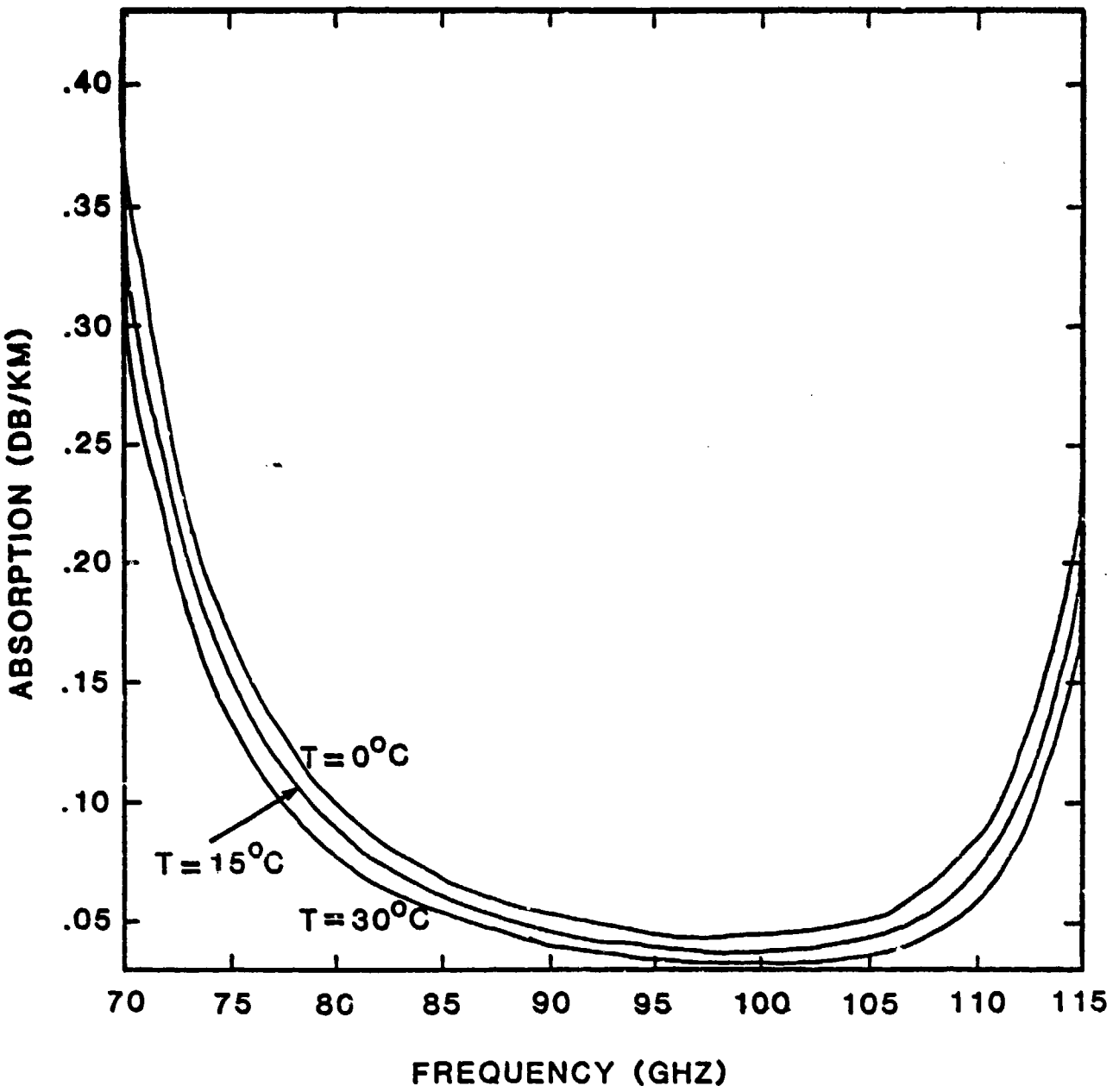

Figure 2-1. Oxygen Absorption Predicted by the LIEBE Model at T=0,15,30°C, F=[70,115] GHz.

Another representation of the O_2 absorption temperature dependance is depicted in Figure 2-2. For both models, it is observed that the decrease of oxygen absorption with temperature is greater at window end frequencies (f=70 and 115 GHz) and smaller near the center of the window (f=94 GHz).

Differences in the LIEBE and EOSAEL model predictions for O_2 absorption are shown in Figure 2-3. The absolute difference between the two models does not exceed .01 db/km for the 70-115 GHz window. As one observed in the previous figure, oxygen absorption values predicted by the EOSAEL model exceed those of the LIEBE model, except near lower frequency (at T>15°C) and upper frequency window bounds. Additionally, the calculated O_2 absorption differences between the two models exhibit the largest range over temperature at the lowest frequency and the smallest range near the upper frequency limit.

The two most obvious differences between the LIEBE and EOSAEL oxygen absorption prediction schemes are the number of oxygen resonance lines and the dry air continuum spectra term used by the LIEBE model. As previously mentioned, the six extra absorption lines in the LIEBE model had no impact on the model predictions within the 70-115 GHz window at the chosen surface conditions. The dry air continuum has a value of ~.005 db/km over the entire frequency range. Since differences between the LIEBE and EOSAEL model predictions are not constant over the frequency window (see Figure 2-3), this term (N_p) cannot explain the observed differences. This would indicate that differences

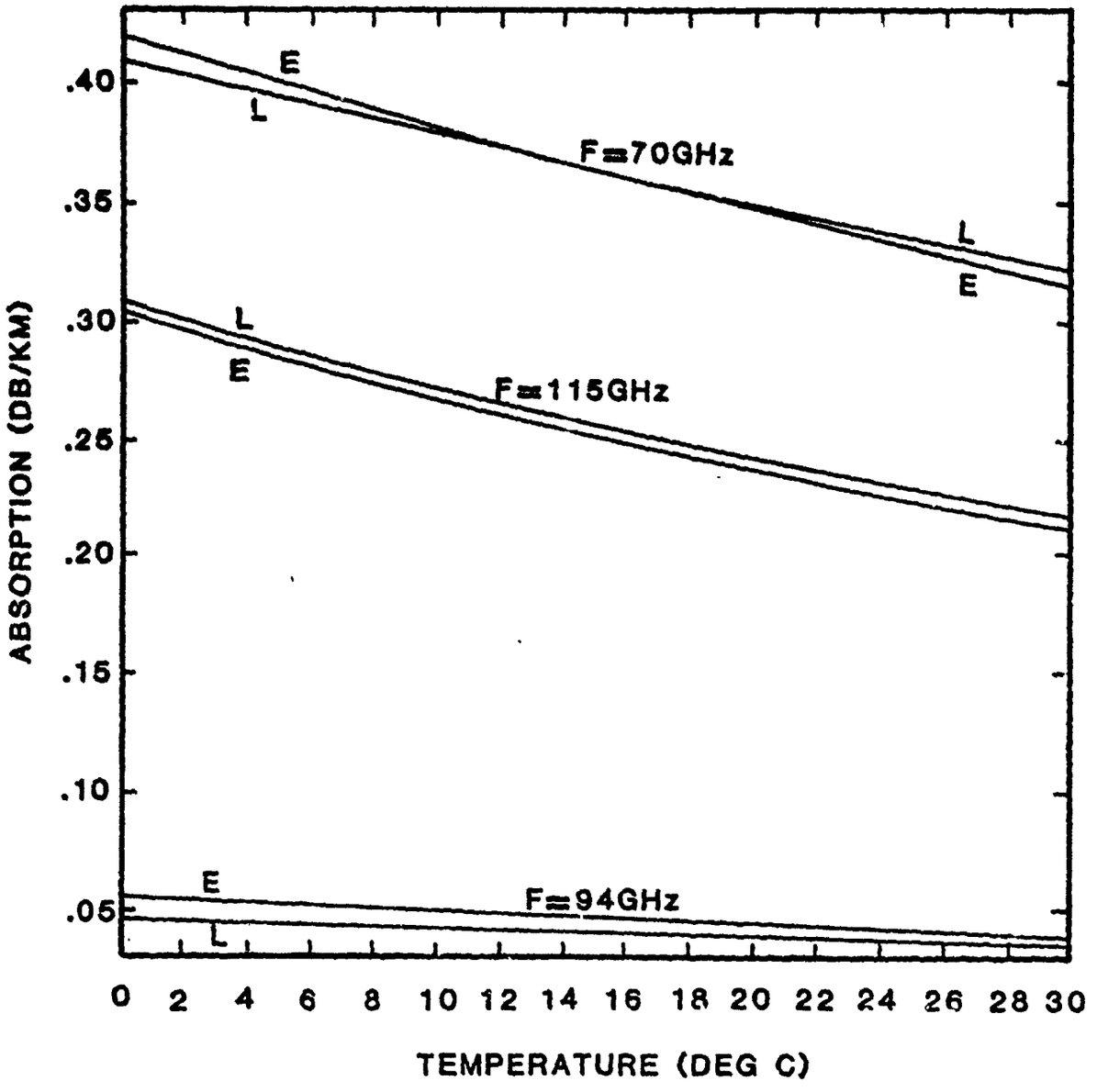

Figure 2-2. Oxygen Absorption Predicted by the LIEBE and EOSAEL Models at F=70,94,115 GHz, T=[0,30]^{o}C.

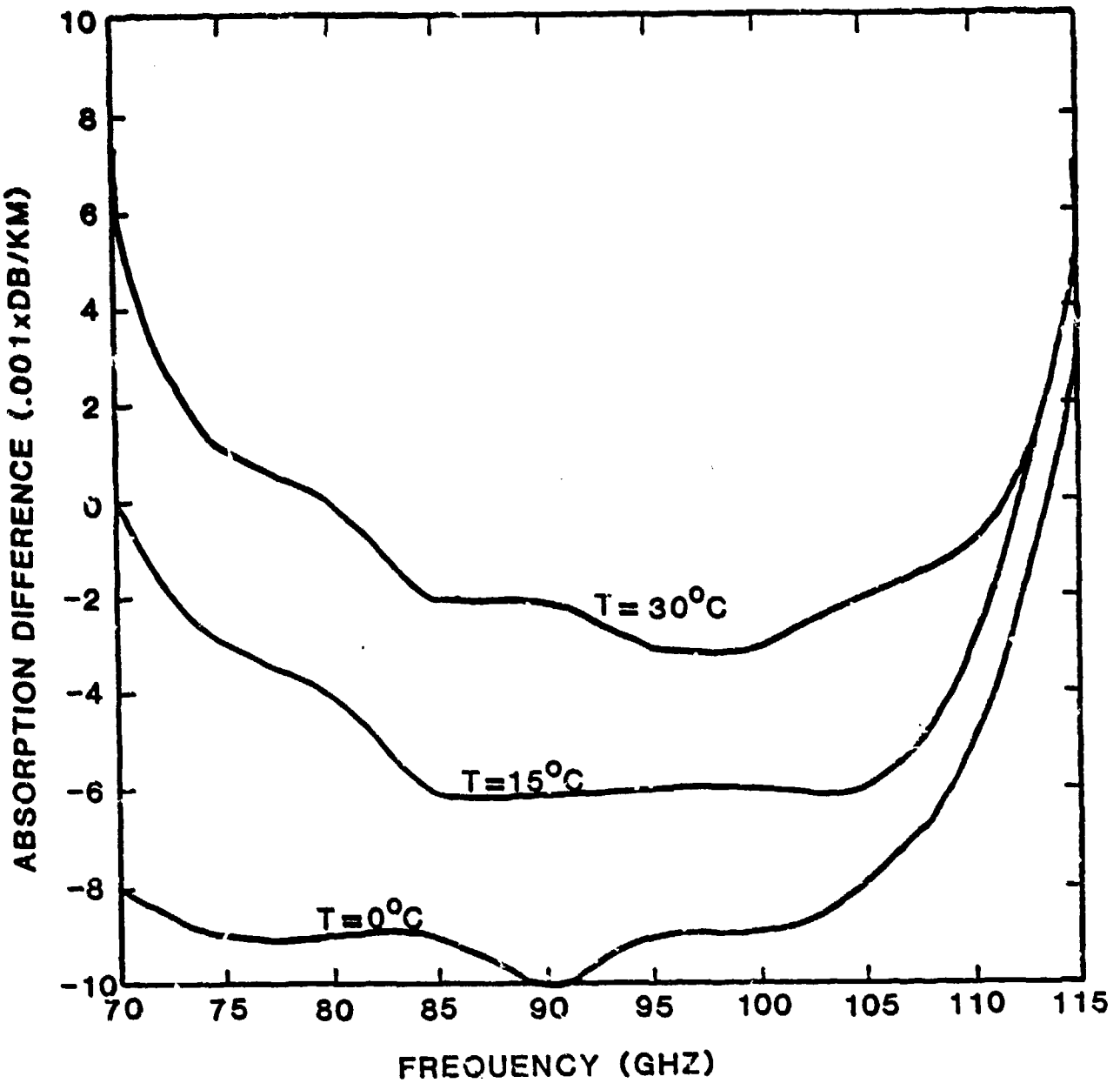

Figure 2-3. Oxygen Absorption Difference (LIEBE-EOSAEL Model Predictions) at T=0,15,30°C, F=[70,115] GHz.

in line strengths and line profile parameters are important factors in O_2 absorption prediction differences between the two models.

2.2.2 Water Vapor Absorption

Analogous to the case for oxygen absorption, the LIEBE model considers absorption due to water vapor to be a sum of absorption due to selected resonance lines and an empirically derived water vapor continuum spectra. Specifically, water vapor absorption (in db/km) is defined as

$$\alpha_{H_2O}(f) = .182f \left[\sum_{i=1}^{n} (S_i F_i) + N_e \right] \qquad (3)$$

where f is the frequency (GHz), n is the number of resonant water vapor lines, S_i is the strength of the ith line, F_i is the line profile for the ith line, and N_e is a water vapor continuum spectra. The terms $S_i F_i$ and N_e are given in ppm. As for the case of O_2 absorption, the LIEBE model employs a modified Van Vleck-Weisskopf form in the calculation of the water vapor line profiles F_i (see equation (2)), and empirical formulations for the line strengths S_i and the line profile parameters (Liebe, 1985a).

The number of resonant water vapor lines utilized by the LIEBE model is 30, all within the frequency range 22-988 GHz. Included in this group are two very weak lines (f=67.8 and 120.1 GHz) just outside the extremes of the window under consideration, another at 22.2 GHz, and a strong absorption line at 183.3 GHz. The remaining lines, at frequencies >300 GHz, vary greatly in strength.

The water vapor continuum spectra, N_e, is derived empirically by fitting experimental data and is given by

$$N_e(f) = [b_f p + b_e e\theta^3]\ fe\theta^{2.5} \qquad (4)$$

where f is the frequency (GHz), $b_f = 1.40 \times 10^{-6}$, $b_e = 5.41 \times 10^{-5}$, p is the dry air pressure and e is the partial water vapor pressure (both in kPa), and θ is a relative inverse temperature ($\theta = 300/T$, T given in ^{o}K).

Model predictions for this water vapor continuum are given in Figure 2-4 for selected temperatures at a relative humidity of 50%. Continuum absorption is observed to increase monotonically with frequency. The values depicted in this graph are very significant; indeed, a comparison with the "total" water vapor absorption predicted by the LIEBE model (Figure 2-5) indicates that the contribution due to the water vapor continuum absorption is dominant, being approximately 80% of the "total" model prediction! This, of course, means that only about 20% of predicted model absorption is due to the 30 selected water vapor resonance lines.

Unlike the LIEBE model, which depends heavily on a continuum spectra to predict water vapor absorption, the EOSAEL model only relies on the summed contributions of water vapor resonance lines to give the total absorption at a given frequency. Specifically, the EOSAEL model defines water vapor absorption as

$$\alpha_{H_2O}(\nu) = \sum_{i=1}^{n} S_i\ C_s(T)\ W(\text{species})\ F_i(\nu, \nu_i, \gamma_i) \qquad (5)$$

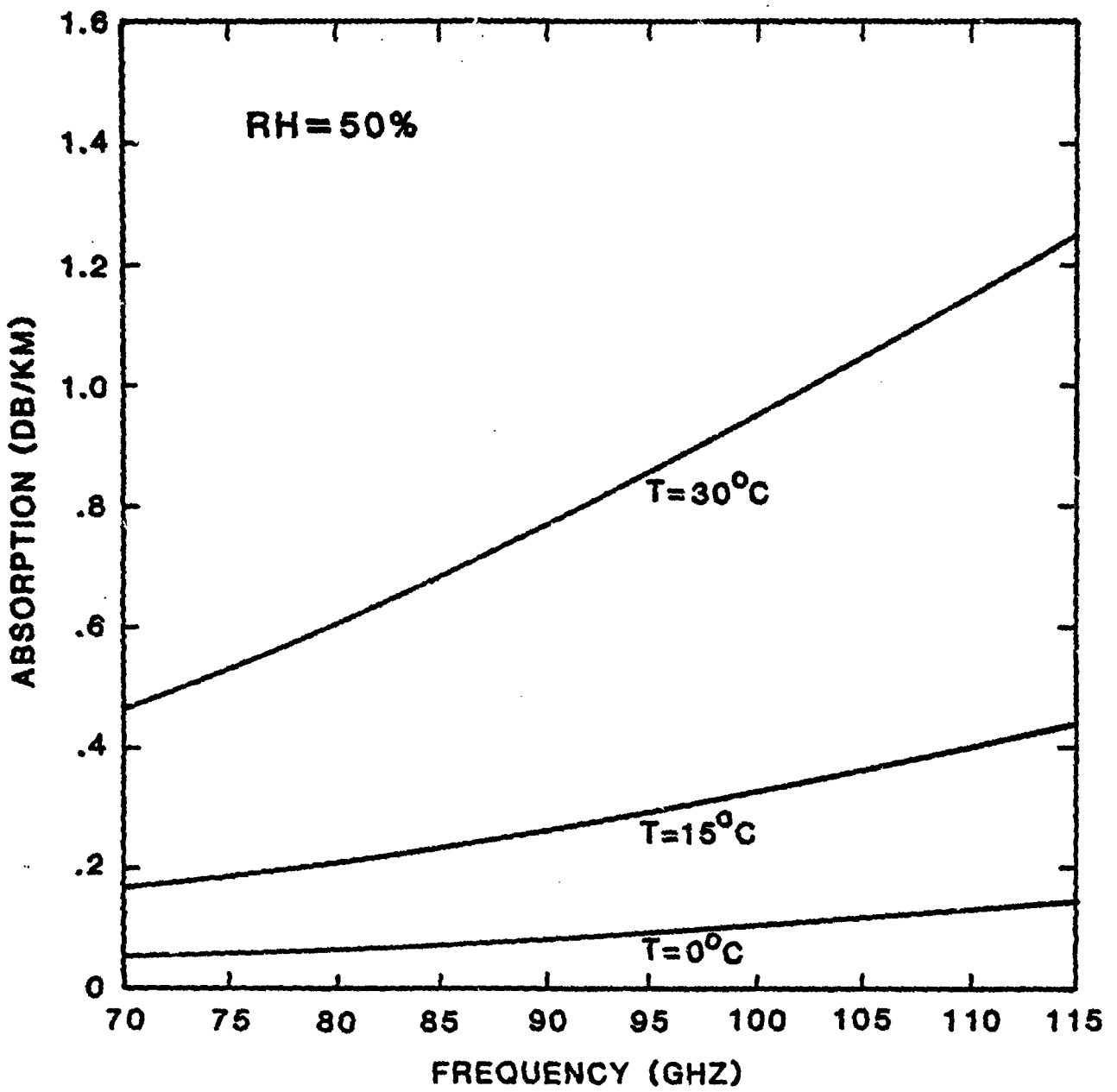

Figure 2-4. LIEBE Model Water Vapor Continuum Absorption Predictions at T=0,15,30°C, F=[70,115] GHz, for a Relative Humidity of 50%.

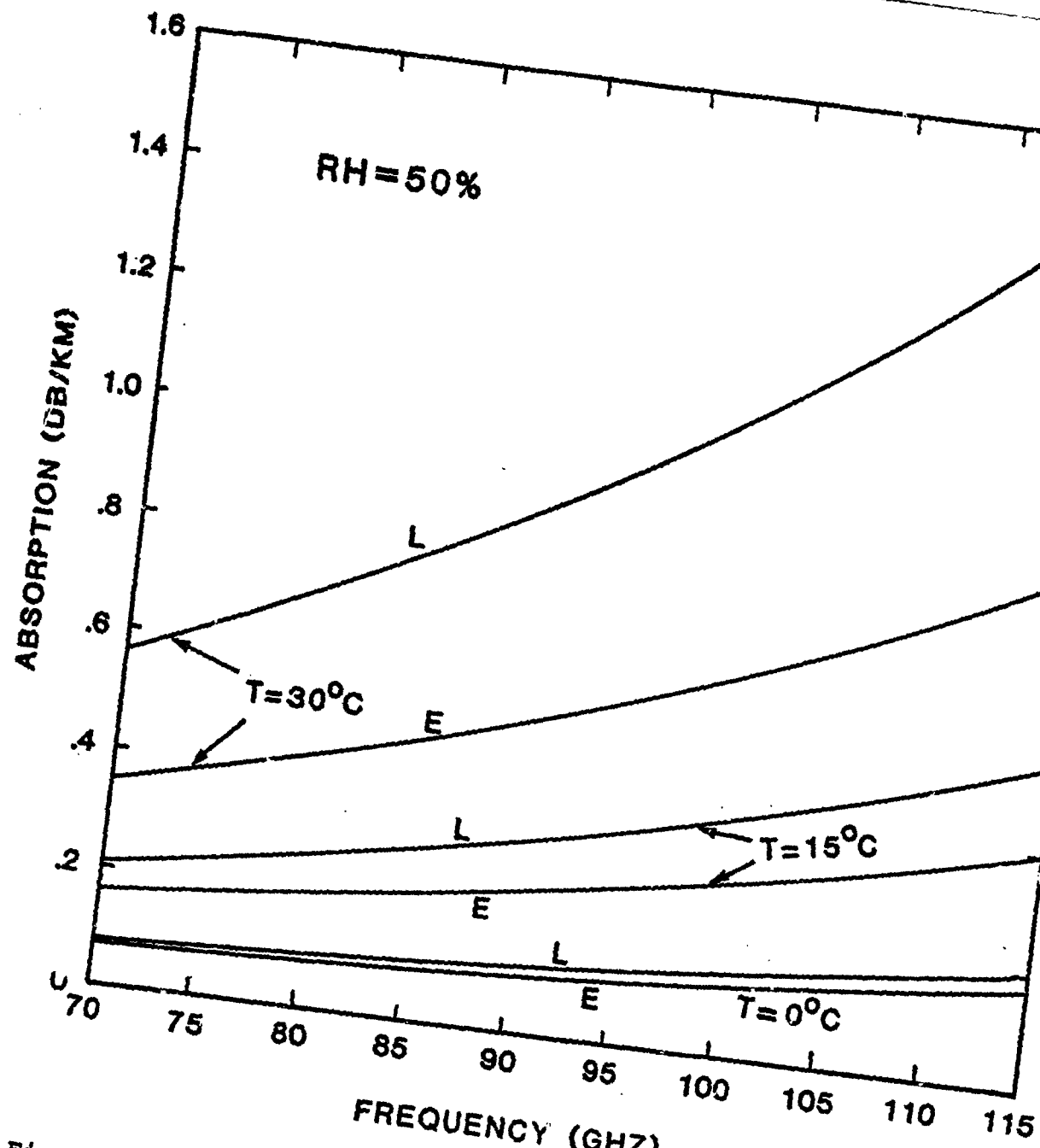

Figure 2-5. Water Vapor Absorption Predicted by the LIEBE and EOSAEL Models at T=0,15,30°C, F=[70,115] GHz, for a Relative Humidity of 50%.

where ν is the wavenumber, n is the number of water vapor resonance lines, S_i is the strength of the ith line, $C_s(T)$ is a temperature correction factor for the line strength, W(species) is the column density for the given species and F_i is the line profile for the ith line.

The EOSAEL model includes 56 absorption lines over the frequency range 22 to 2264 GHz, selected on the basis of their strength (Brown, 1984). This selection does not include lines at f=67.8 and 120.1 GHz which are used in the LIEBE model. The water vapor absorption lines at 22.2 and 183.1 GHz are included in the EOSAEL formulation.

The line profile employed in the EOSAEL model prediction of water vapor absorption is distinct from that used for oxygen absorption. The profile is defined as

$$F_i(\nu, \nu_i, \gamma_i) = \frac{NORM}{\pi\gamma_i}\left[\left(\frac{\nu_i^2-\nu^2}{2\gamma_i\nu}\right)^2 + 1\right]^{-1} \qquad |\nu-\nu_i| \leq \Delta\nu \qquad (6a)$$

and

$$F_i(\nu, \nu_i, \gamma_i) = \frac{NORM}{\pi\gamma_i} X\left[\left(\frac{\nu_i^2-\nu^2}{2\gamma_i\nu}\right)^{1.88} + 1\right]^{-1} \qquad |\nu-\nu_i| > \Delta\nu \qquad (6b)$$

where ν is the wavenumber, ν_i is the center wavenumber for the ith line, γ_i is the pressure and temperature corrected ith line half-width, NORM is a normalization parameter and X is defined such that F_i is continuous at $\nu \pm \nu_i = \Delta\nu$, with $\Delta\nu = 10\gamma_i$.

Figure 2-5 gives a comparison of the LIEBE and EOSAEL model predictions for water vapor absorption at a relative humidity of 50%. For the chosen temperature and frequency range, the model predictions are most similar at the lowest temperature and frequency ($T=0^{o}C$, f=70 GHz) and most deviate at the highest temperature and frequency ($T=30^{o}C$, f=115 GHz). In all cases, the LIEBE model predictions exceed the EOSAEL model predictions, being from 10% to 70% greater.

Figures 2-6 and 2-7 depict the temperature dependence of the water vapor absorption slope at 94 GHz for the EOSAEL and LIEBE models, respectively. The absorption slope, defined as the water vapor absorption divided by the absolute humidity v, is shown at selected absolute humidities (v=1 to 20g/m^3) and relative humidities (RH=10 to 100%). For the EOSAEL model, the water vapor absorption slope is observed to be inversely proportional to temperature for both absolute and relative humidities. In the LIEBE model predictions, the negative temperature dependence for absorption slope is noted for absolute humidity but only at low relative humidities (viz. RH=10%). At higher relative humidities, the absorption slope becomes increasingly more positive with temperature. This strong positive temperature dependence at high relative humidities is due to the square vapor pressure term in the water vapor continuum formulation (Liebe, 1985a).

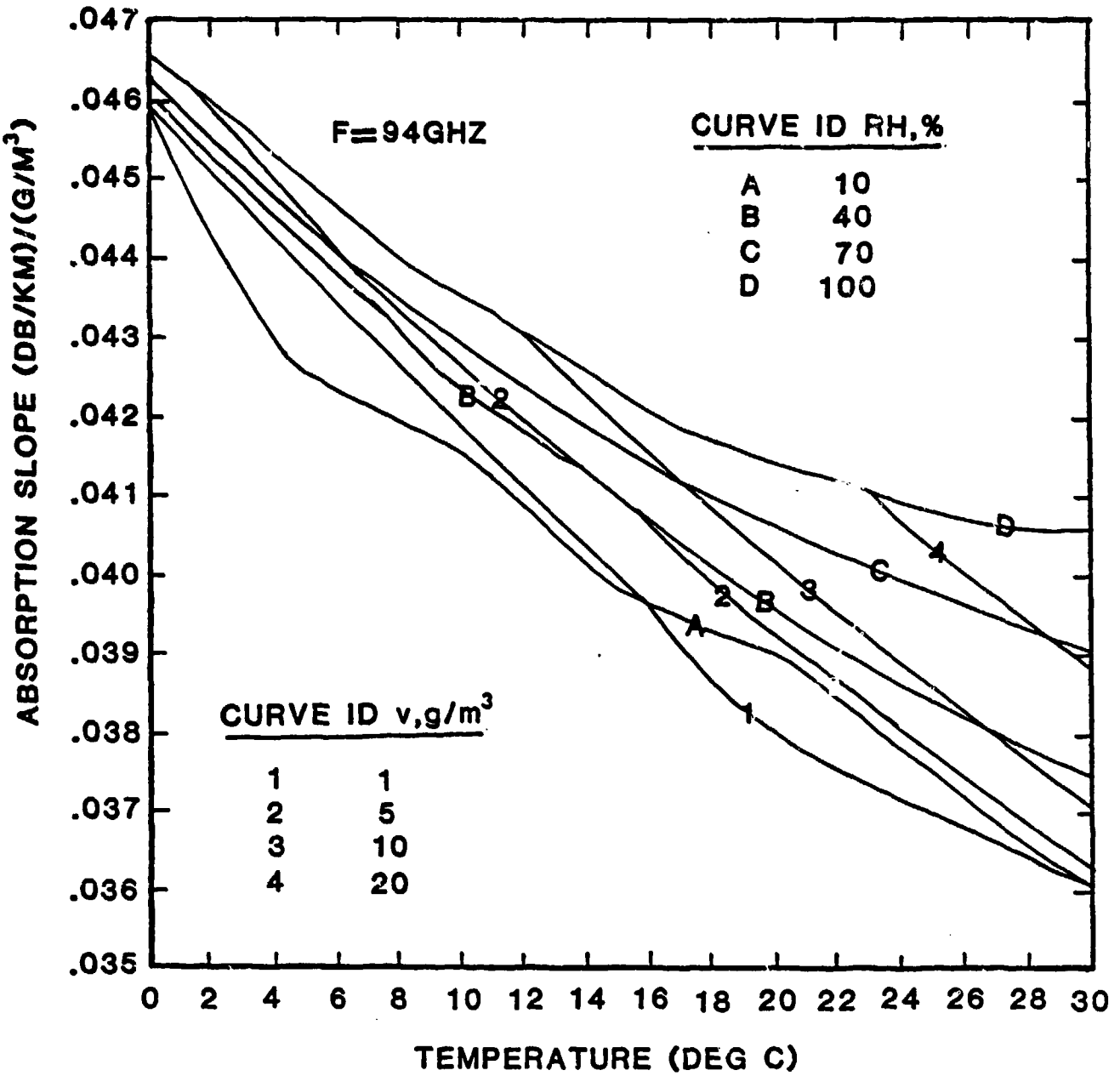

Figure 2-6. Water Vapor Absorption Slope Predicted by the EOSAEL Model at F=94 GHz, T=[0,30]°C, for Selected Absolute and Relative Humidities.

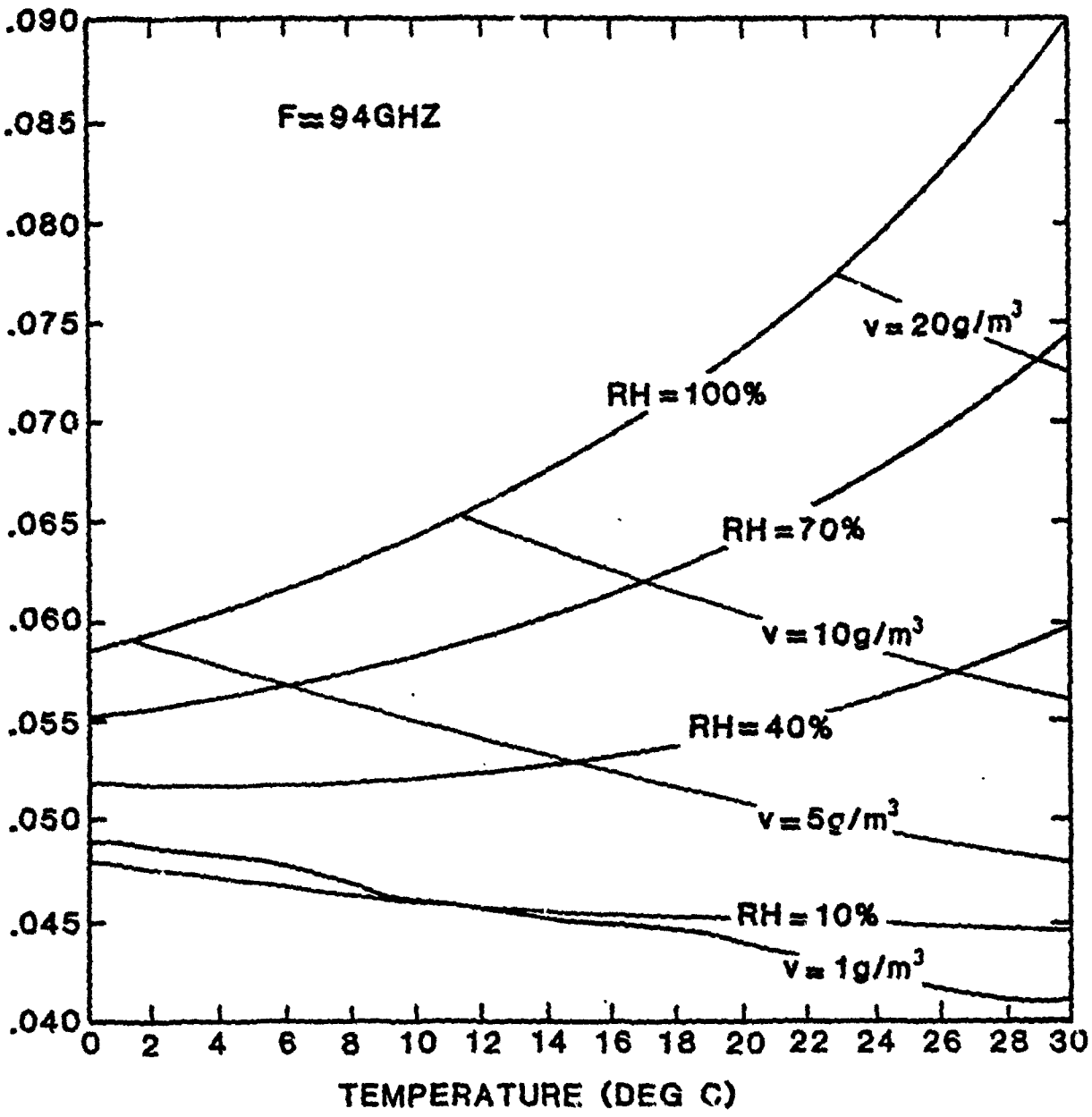

Figure 2-7. Water Vapor Absorption Slope Predicted by the LIEBE Model at F=94 GHz, T=[0,30]°C, for Selected Absolute and Relative Humidities.

2.2.3 Gaseous Absorption

Near the earth's surface, gaseous absorption is considered due only to molecular oxygen and water vapor. Absorption by ozone, of some importance at high altitudes, is negligible at the surface and is considered by neither the LIEBE (tropospheric) nor the EOSAEL model.

Figure 2-8 presents the gaseous absorption predicted by the LIEBE and EOSAEL models at selected temperatures for a relative humidity of 50%. At T=0°C, the model predictions are quite close over the entire frequency window. At T=30°C, the model differences are substantial, with the LIEBE model gaseous absorption predictions 30% to 60% greater than those of the EOSAEL model. For both models, the minimum predicted gaseous absorption shifts towards lower frequencies with increasing temperature (and absolute humidity). Specifically, the minimum predicted gaseous absorptions occur near 90 GHz at T=0°C and between 75 and 80 GHz at T=30°C.

Gaseous absorption model predictions as a function of temperature, at RH=50% and selected frequencies, are shown in Figure 2-9. The differences in the LIEBE and EOSAEL model predictions are seen to increase considerably with temperature. For both models, the positive absorption slopes are observed to steepen with increased frequency.

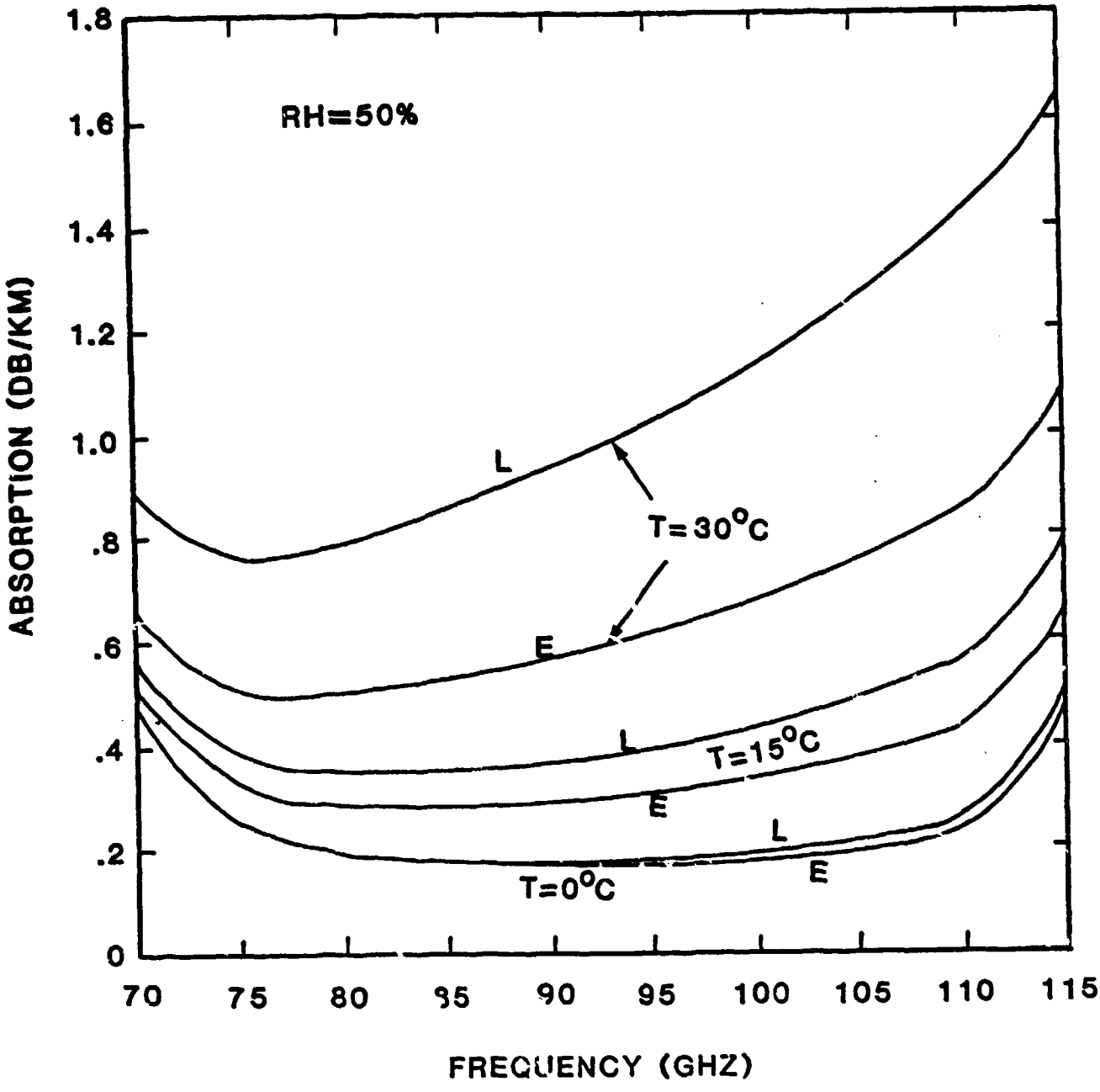

Figure 2-8. Gaseous Absorption Predicted by the LIEBE and EOSAEL Models at T=0,15,30°C, F=[70,115] GHz, for a Relative Humidity of 50%.

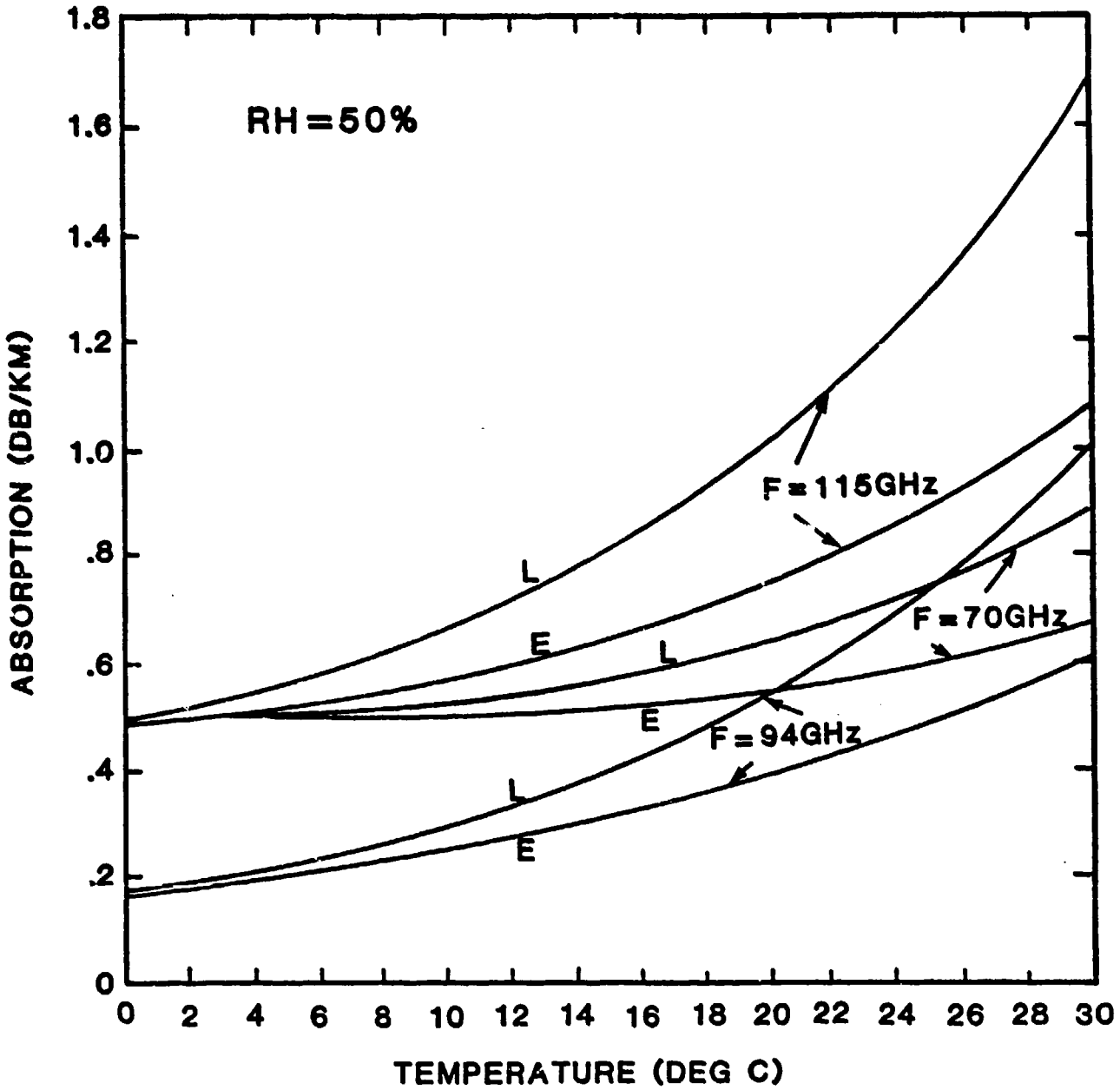

Figure 2-9. Gaseous Absorption Predicted by the LIEBE and EOSAEL Models at F=70,94,115 GHz, T=[0,30]°C, for a Relative Humidity of 50%.

2.3 Hydrometeor Effects

2.3.1 Fog Attenuation

The theories used by the LIEBE and EOSAEL models to calculate suspended liquid water (i.e., fog or cloud) attenuation are essentially identical. With small aerosol sizes below 50 μm, the Rayleigh approximation of Mie scattering theory can be applied, such that the specific attenuation due to fog (in db/km) may be expressed as

$$\alpha_{FOG}\ (f) = .273fw\ IM\left(-\frac{m^2-1}{m^2+2}\right) \qquad (7)$$

where f is the frequency (GHz), w is the liquid water content (g/m^3), m is the complex index of refraction for water ($m=n_r - in_i$) and IM denotes the imaginary part.

With the frequency and liquid water content designated on input, any differences in fog predictions by the LIEBE and EOSAEL models can only be ascribed to the differences in the empirical formulations applied for the calculation of the complex index of refraction. For both models, this refractive index is given in terms of the complex permittivity $\varepsilon = (\varepsilon' - i\varepsilon'')$, where ε' is the dielectric constant for water and ε'', the loss. These are related to the complex index of refraction by

$$\varepsilon' = n_r^2 - n_i^2 \quad \text{and} \quad \varepsilon'' = 2n_r n_i \qquad (8)$$

The dielectric data ε', ε'' are calculated in the LIEBE model with the Debye formulae as reported by Chang and Wilheit (1979), and are calculated in the EOSAEL model based on the Debye model formulation given by Ray (1972).

Figure 2-10 depicts the liquid water attenuation at various temperatures over the frequency range 70-115 GHz, as predicted by the LIEBE and EOSAEL models. A value of 0.5 g/m^3 is assigned for the liquid water content. This value exceeds the maximum expected for advection fog ($w=0.4\ g/m^3$) but is less than the maximum expected for radiation fog ($w=1.0\ g/m^3$) (Koester and Kosowsky, 1970), and is used for model comparisons to accentuate differences. Liquid water attenuation is observed to be monotonically increasing with frequency over the 0-30°C temperature range, with higher values of attenuation at lower temperatures. LIEBE model predictions exceed those for the EOSAEL model over the entire temperature range, being approximately 5% to 7% greater.

Model predictions of attenuation versus temperature, at 94 GHz and selected liquid water concentrations, are shown in Figure 2-11. For both models, liquid water attenuation is observed to monotonically decrease with temperature, with the rate of decrease, increasing with greater liquid water content. Although the LIEBE model predictions exceed those of the EOSAEL model over the range $w=0.1$ to $1.0\ g/m^3$, the exceedence is fairly constant (~5.5%) over temperature.

The strong influence of liquid water content on attenuation is displayed in Figure 2-12. In this graph, attenuation is given for several frequencies at a temperature of 15°C. For both models, it is noted that attenuation is a linear function of liquid water content at all frequencies. Significant attenuation

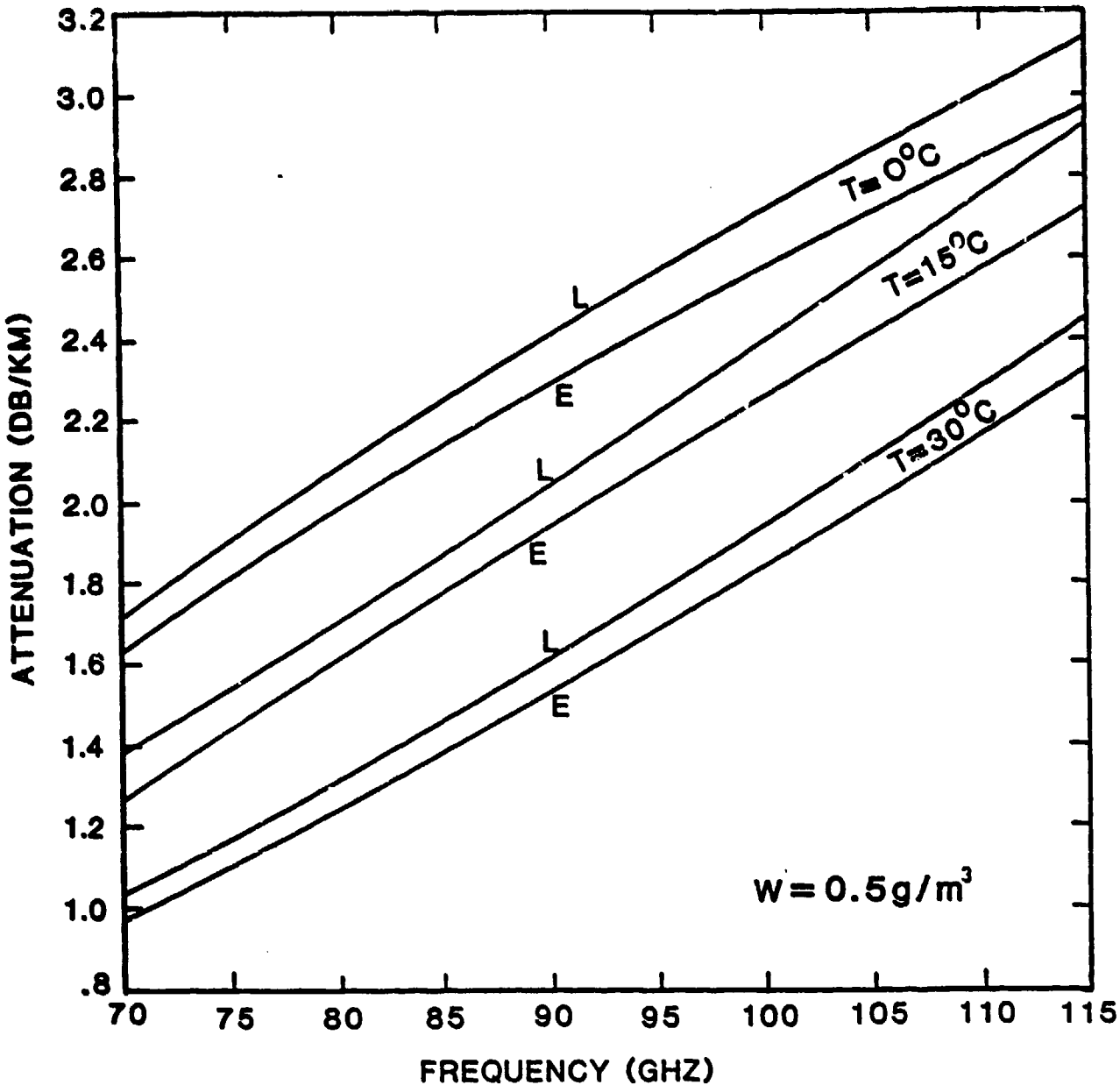

Figure 2-10. Liquid Water Attenuation Predicted by the LIEBE and EOSAEL Models at T=0,15,30°C, F=[70,115] GHz, for a Liquid Water Content w= 0.5 g/m³.

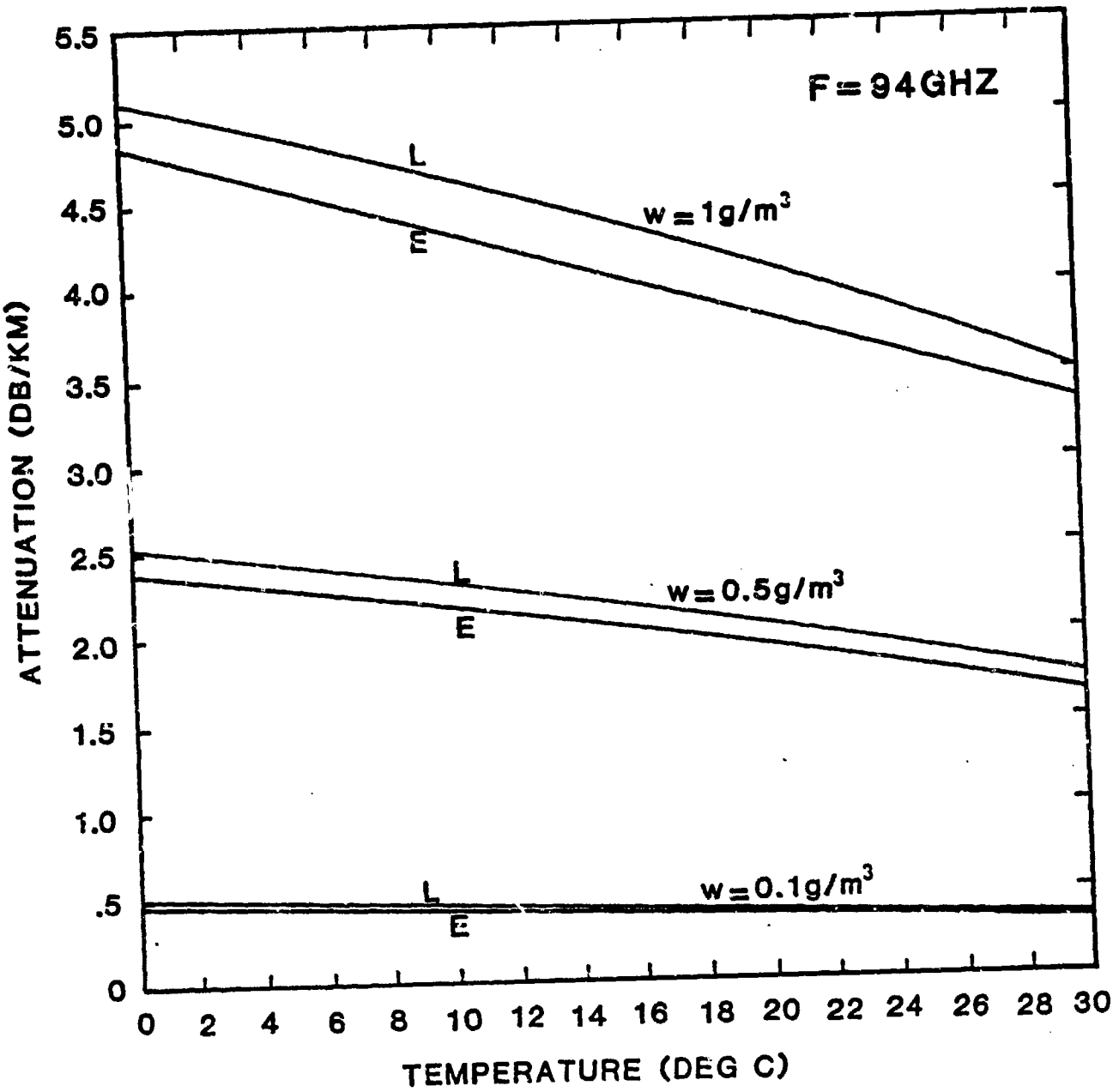

Figure 2-11. Liquid Water Attenuation Predicted by the LIEBE and EOSAEL Models at F=94 GHz, T=[0,30]°C, and w=0.1,0.5,1.0 g/m^3.

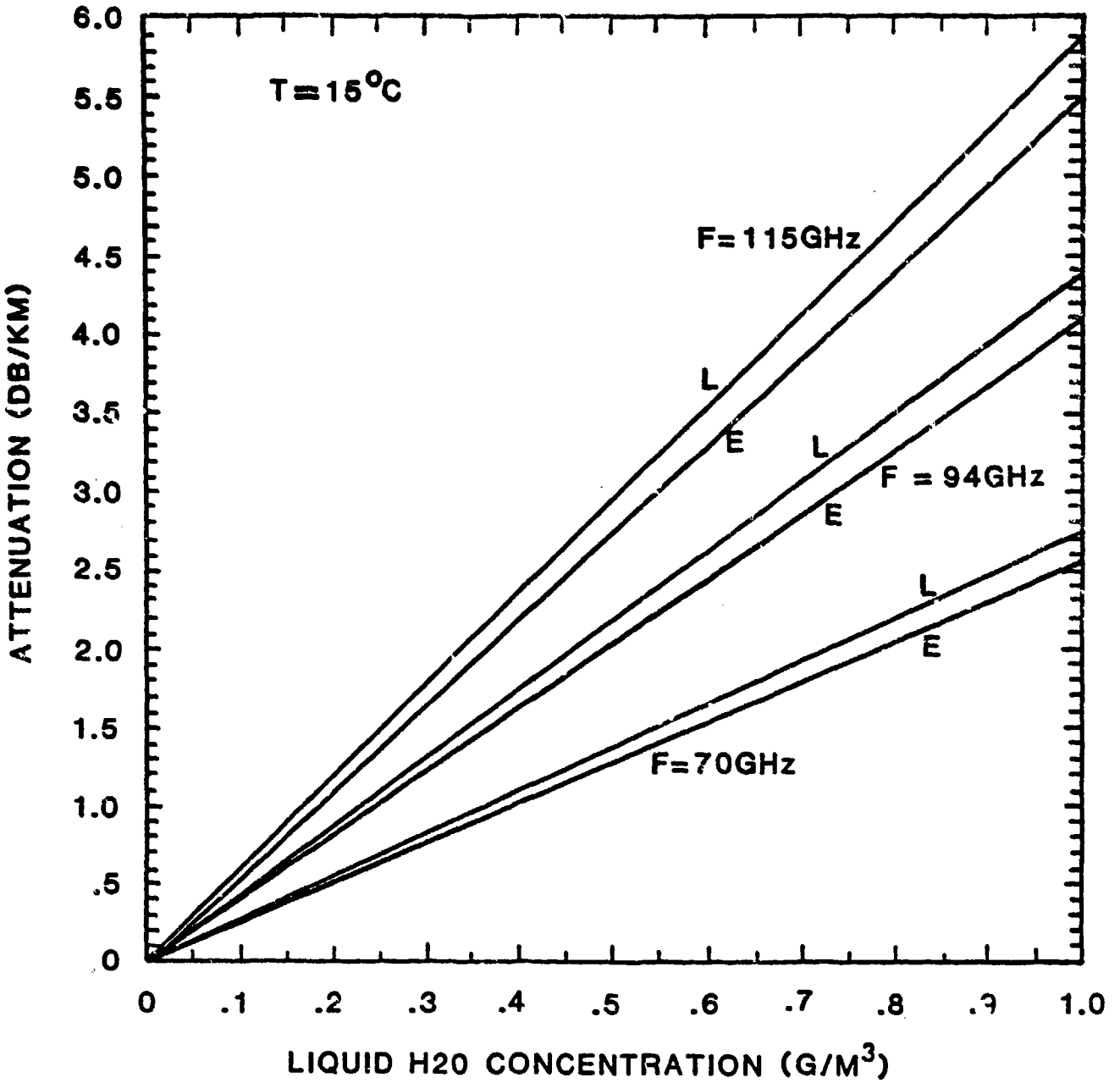

Figure 2-12. Liquid Water Attenuation Predicted by the LIEBE and EOSAEL Models at T=15°C, w=[0,1] g/m^3, and F=70,94,115 GHz.

values are predicted by both models for large liquid water content. At w=1.0 g/m^3, a value obtained in a very dense radiation fog or within a cumulus cloud, specific attenuation ranges from approximately 2.5 to 5.5 db/km. For typical radiation and advective fog liquid water contents of 0.11 g/m^3 and 0.17 g/m^3 (Koester and Kosowsky,1970), the predicted attenuation range is much smaller over 70-115 GHz, from about 0.5 to 0.7 db/km.

2.3.2 Rain Attenuation

Raindrop sizes are too large to allow a Rayleigh approximation of Mie scattering theory to be used in the calculation of rain attenuation. Although the validity of the Mie scattering theory is well established, its complexity is not well suited for rain attenuation modeling. As a substitute, an empirical procedure based on an approximate relation between the attenuation and the rainfall rate is widely used (Olsen et al., 1978). This power law relation, also utilized by the LIEBE and EOSAEL models, takes the form

$$A = aR^b \tag{9}$$

where A is the rain attenuation (db/km), R is the rainfall rate (mm/hr), and a and b are functions of frequency f and, for the EOSAEL model, rain temperature T.

The calculation of rain attenuation requires the specification of a dropsize distribution. The LIEBE model uses a Laws and Parsons (LP) distribution, while the EOSAEL model uses three; the Marshall and Palmer (MP) distribution (for widespread rain), and the Joss drizzle and thunderstorm distributions. All of these distributions are described in some detail by Olsen et al. (1978).

The essential difference between the LP and MP distributions is in the number of small drops, with the MP distribution containing significantly more small drops than the LP distribution. This is important for attenuation in that smaller drops, with relatively larger surface area to volume ratios, produce greater attenuation rates. The Joss drizzle (thunderstorm) distribution has a predominance of small (large) drops, which gives an upper (lower) bound for the mean expected rain attenuation of the MP distribution.

For both models, the values for a and b are computed by applying logarithmic regression to Mie scattering calculations. In the LIEBE model, with the assumptions of a LP dropsize distribution and a rain temperature of $0^{\circ}C$, the coefficients a and b are computed for the frequency range 70-115 GHz by the equations:

$$a(f) = .0409f^{0.669} \tag{10a}$$

$$b(f) = 2.63f^{-0.272} \tag{10b}$$

The EOSAEL model contains tabular values for the coefficients a and b, calculated by logarithmic interpolation over three rain temperatures ($-10, 0, 20^{\circ}C$) and 17 frequencies from 10-1000 GHz. In recognition that the coefficients a and b are relatively unvarying at smaller rainrates, the coefficients are chosen by the EOSAEL model at a rainrate of 2.5 mm/hr for the Joss drizzle distribution, at 4.0 mm/hr for the MP (widespread) distribution, and at 25 mm/hr for the Joss thunderstorm distribution.

Figure 2-13 shows the LIEBE and EOSAEL (widespread rain type) model predictions of rain attenuation at low rainrates (0.2 to 5.0 mm/hr), for a rain temperature of 0°C. The EOSAEL model predictions are larger than those of the LIEBE model at all rainrates displayed over the frequency range 70-115 GHz, with the differences between models greater at higher frequencies. Whereas the slope of rain attenuation versus frequency is nearly linear at rainrates 0.2 to 5.0 mm/hr for the LIEBE model, the EOSAEL model predictions (>1.0 mm/hr) show a more rapid increase of attenuation with frequency at lower frequencies (~<95 GHz) than at higher frequencies.

LIEBE and EOSAEL (widespread rain type) model attenuation predictions at moderate to heavy rainrates (12.5 to 100 mm/hr), and a rain temperature of 0°C, are depicted in Figure 2-14. EOSAEL model predictions are seen to exceed those of the LIEBE model, with the differences greater at higher frequencies. At very high rainfall rates (50-100 mm/hr), predicted LIEBE model rain attenuation decreases with increasing frequency, reversing the tendency to increase with frequency, as observed at lower rainfall rates. Only at the highest rainfall rate (100 mm/hr) does the EOSAEL model predict a decrease of attenuation with frequency, and this at frequencies >95 GHz.

The effect of variations in rain temperature are not modeled by Liebe; resultingly, LIEBE model rain attenuation predictions are constant with temperature. The logarithmic temperature interpolation scheme employed by the EOSAEL model results in

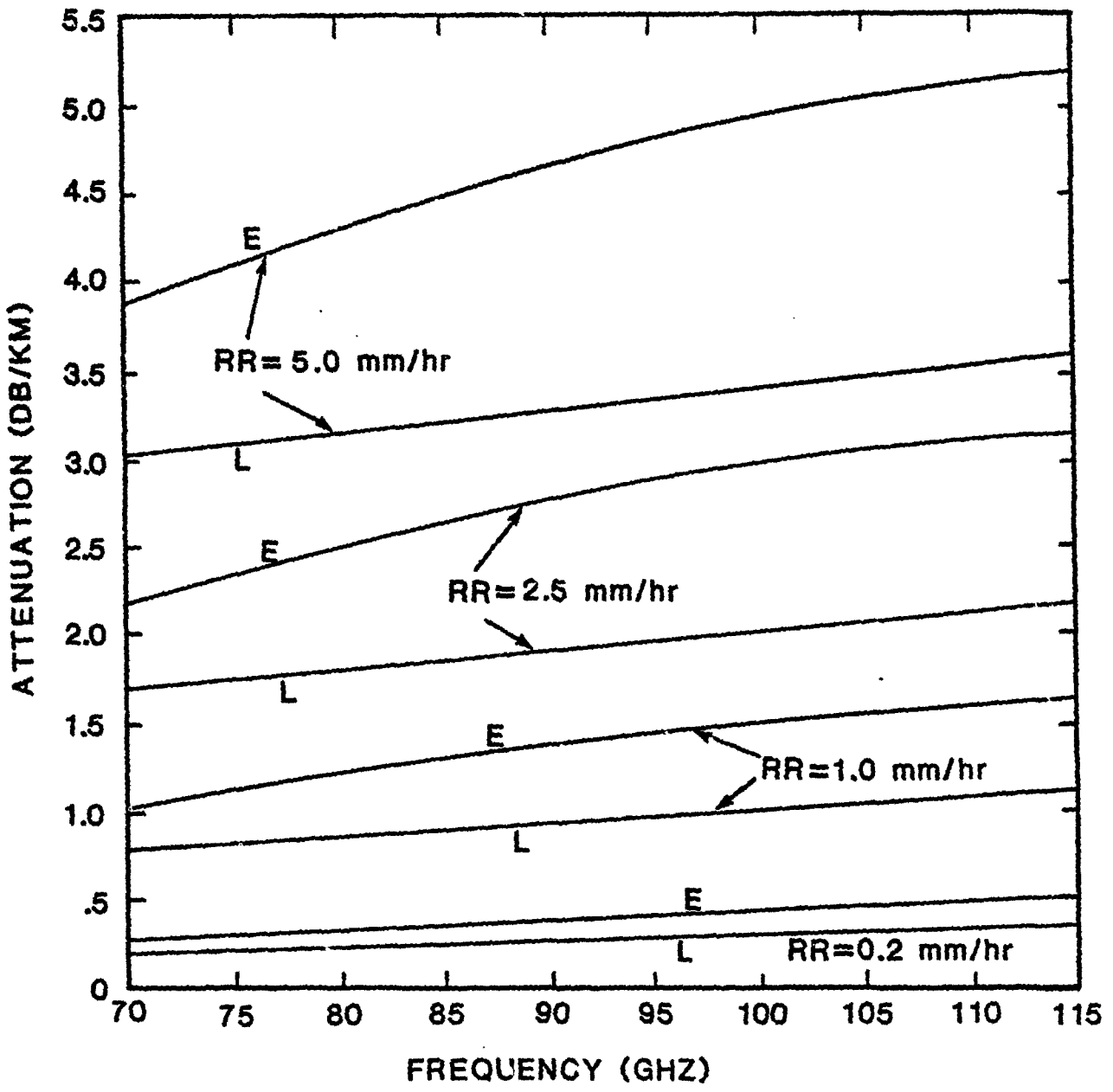

Figure 2-13. Rain Attenuation Predicted by the LIEBE and EOSAEL Models at Light to Moderate Rainfall Rates over the Frequency Range 70-115 GHz, for a Rain Temperature of 0°C.

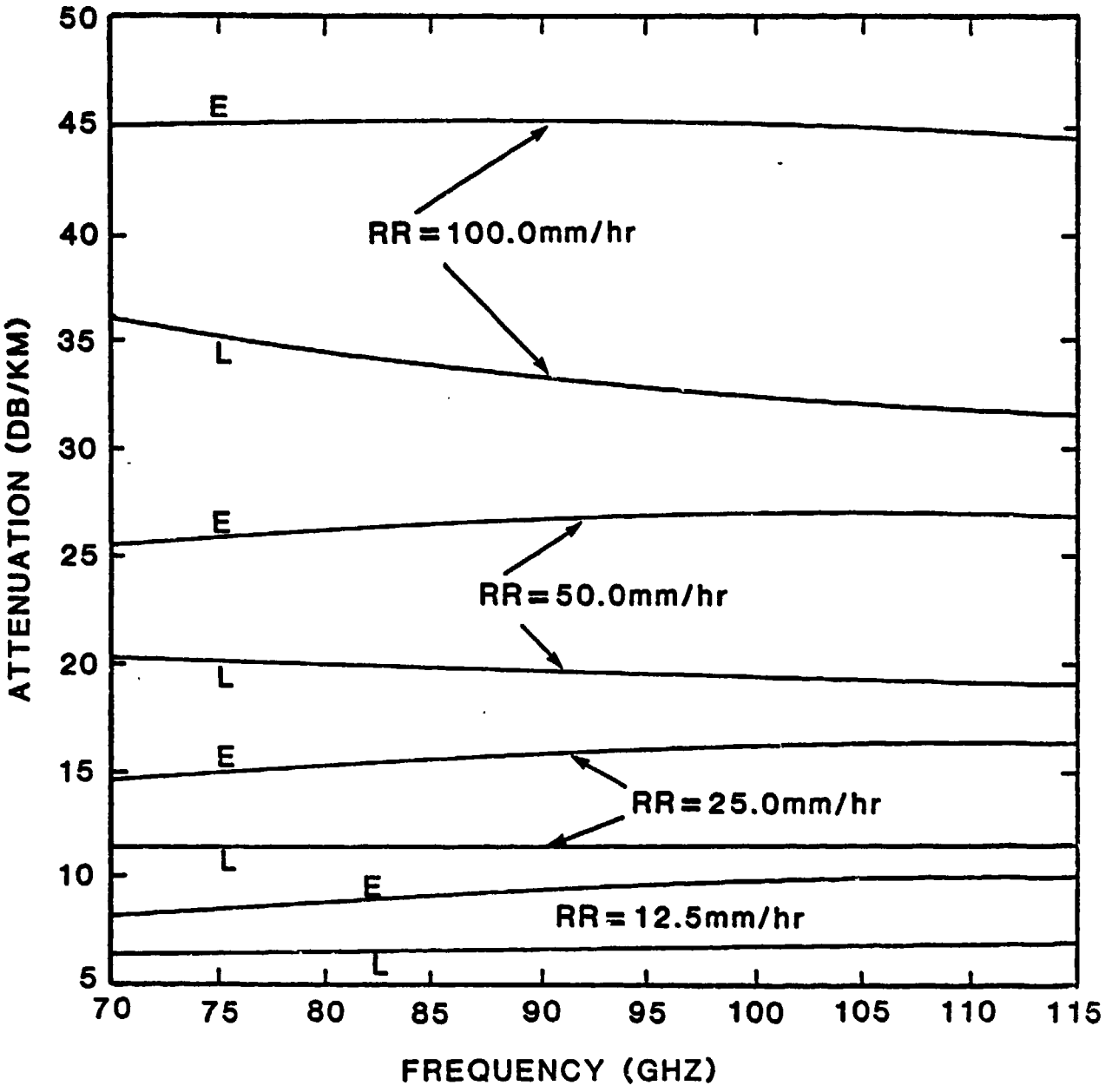

Figure 2-14. Rain Attenuation Predicted by the LIEBE and EOSAEL Models at Moderate to Heavy Rainfall Rates over the Frequency Range 70-115 GHz, for a Rain Temperature of 0°C.

only a slight dependence of rain attenuation on temperature at T < 20°C. Specifically, at a frequency of 94 GHz, a slight increase of attenuation with temperature is predicted at light to moderate rainfall rates over the range 0-20°C, and a slight decrease in attenuation is predicted at high rainfall rates over the same temperature range.

3. VERIFICATION OF MODELS

In this section, the LIEBE and EOSAEL model predictions of attenuation due to molecular oxygen, water vapor, fog and rain, are compared with available measurements from the literature. It should be emphasized that measurements found in the literature are of a varying degree of reliability, are in many cases not well documented as to precision and accuracy, and most often are presented in graphical form, especially log-linear. These factors, along with the simplifying approximations used in modeling, make a quantitative assessment of model verification with observations inappropiate. Thus, the emphasis in this section will be on the assessment of the qualitative agreement between model prediction and observation.

3.1 Clear Atmosphere Effects

3.1.1 Oxygen Absorption

Measurements of attenuation due to molecular oxygen at millimeter wavelengths are not common in the published literature. For this study, measurements from only three sources, the University of Texas, the Bell Telephone Laboratory, and Gor'kii University, were found for model verification. These measurements, along with the LIEBE and EOSAEL model predictions of

oxygen absorption, are displayed in Figure 3-1. Of the eight measurements shown, only one (number 8) is from a laboratory; the remaining were taken through the actual atmosphere. As can be seen, most of the measurements are near either the lower or upper limit of the frequency range. The model predictions are for a pressure of 1 atm. and a temperature of 300°K. All observations are at a pressure of 1 atmosphere. The laboratory measurement is at a temperature of 300°K; the remaining measurements are believed scaled to 300°K, although neither Straiton and Tolbert (1960) nor Dryagin et al. (1966) state this explicitly.

Several features are apparent in Figure 3-1. First, the LIEBE and EOSAEL model predictions are virtually coincidental; such that, at each frequency with a measurement, the difference between the LIEBE and EOSAEL predictions is much less than the difference between the measurement and either the LIEBE or EOSAEL model prediction. Second, all observations are well in excess of the theoretical predictions, with several measurements near the upper frequency limit 200% to 300% greater than either the LIEBE or EOSAEL model prediction. Such significant differences between observation and theory can hardly be explained on the basis of experimental errors, and lend support to the idea that the theory of molecular oxygen absorption, upon which the LIEBE and EOSAEL models are based, is not completely satisfactory.

3.1.2 Water Vapor Absorption

Figure 3-2 presents the water vapor absorption predicted by the LIEBE and EOSAEL models at a pressure of 1 atm., an absolute humidity of 7.5 g/m^3, and three different temperatures (6.55, 20,

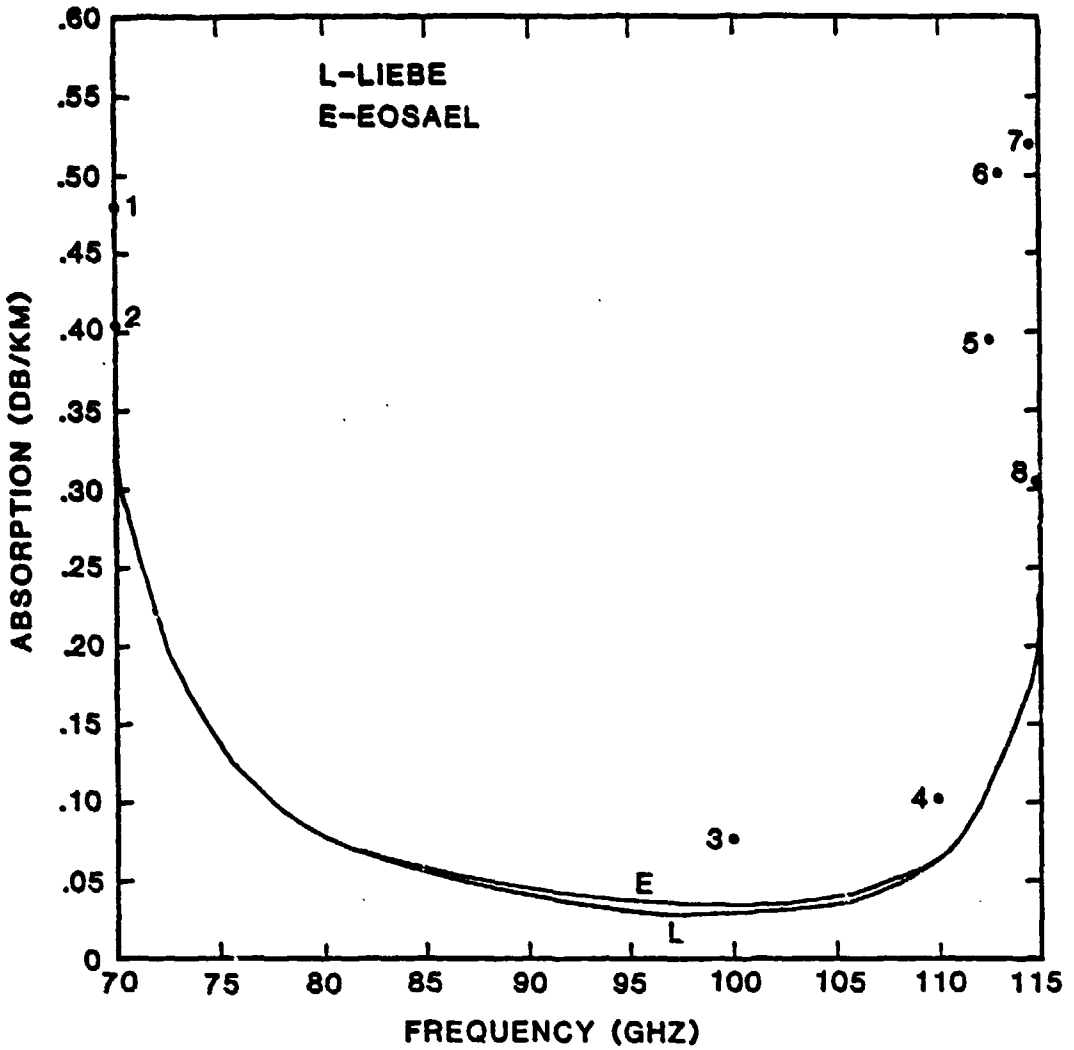

MEASUREMENT		
NO.	SOURCE	REFERENCE
1	University of Texas	Straiton and Tolbert (1960)
2	Bell Telephone Lab.	Straiton and Tolbert (1960)
3	University of Texas	Straiton and Tolbert (1960)
4	University of Texas	Dryagin et al. (1966)
5	University of Texas	Dryagin et al. (1966)
6	Gor'kii University	Dryagin et al. (1966)
7	Gor'kii University	Dryagin et al. (1966)
8	University of Texas	Schulze and Tolbert (1963)

Figure 3-1. Measured and Predicted Oxygen Absorption at T=300°K, p=1 atm., and F=[70,115] GHz.

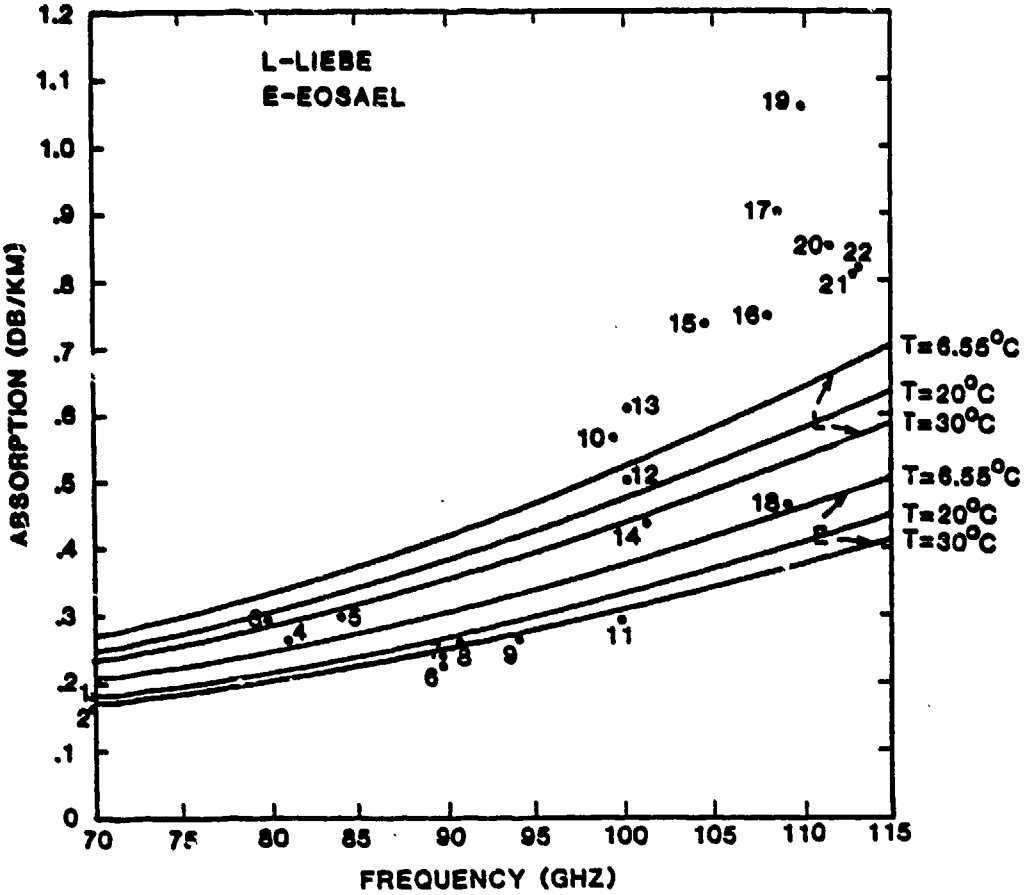

NO.	SOURCE	MEASUREMENT REFERENCE
1	University of Texas	Straiton and Tolbert (1960)
2	Bell Telephone Lab.	Straiton and Tolbert (1960)
3	Appleton Lab.	LIEBE (1980)
4	Bell Telephone Lab.	Straiton and Tolbert (1960)
5	Gor'kii University	Gibbons et al. (1975)
6	University of Texas	Straiton and Tolbert (1960)
7	Queen Mary College	Bastin (1966)
8	Aerospace Corporation	Gibbins et al. (1975)
9	University of Texas	Dryagin et al. (1966)
10	Gor'kii University	Dryagin et al. (1966)
11	University of Texas	Dryagin et al. (1966)
12	Martin Company	Gibbons et al. (1975)
13	University of Texas	Tolbert and Straiton (1961)
14	Georgia Inst. of Tech.	Gibbins et al. (1975)
15	University of Texas	Tolbert and Straiton (1961)
16	Gor'kii University	Dryagin et al. (1966)
17	Gor'kii University	Gibbons et al. (1975)
18	University of Texas	Dryagin et al. (1966)
19	University of Texas	Tolbert and Straiton (1961)
20	Gor'kii University	Dryagin et al. (1966)
21	Gor'kii University	Gibbons et al. (1975)
22	University of Texas	Tolbert and Straiton (1961)

Figure 3-2. Measured and Predicted Water Vapor Absorption at $v=7.5\ g/m^3$, p=1 atm., F=[70,115] GHz, and T=[6.55,30]°C.

and 30°C). The value T=6.55°C corresponds to 100% relative humidity. Also shown are 22 measurements from diverse sources (the vast majority field measurements), obtained by various techniques and apparatus. Each measurement corresponds to a pressure of 1 atmosphere. The measurements reported by Straiton and Tolbert (1960), Dryagin et al. (1966) and Bastin (1966) were scaled, by the respective authors, to an absolute humidity of 7.5 g/m^3 by assuming a linear relation between absorption and absolute humidity. The remaining measurements, reported at 1 g/m^3 absolute humidity, were similarily normalized by this author to 7.5 g/m^3.

Although widely applied in the literature, the use of linearity to normalize water vapor measurements taken at varying humidities appears not to be fully justified. As evidence to this, consider the theoretical results from the LIEBE model as shown in Figure 2-7. In this figure, it is observed that the relation between water vapor absorption and humidity is non-linear; for example, at a temperature of 20°C, the LIEBE model predicts water vapor absorption slopes of ~.0442 and ~.0552 db/km per g/m^3 at 1.0 and 7.5 g/m^3, respectively. This nonlinear dependence of water vapor absorption slope on humidity, as predicted by theory, suggests that inaccuracies likely occur in linear normalization of water vapor absorption data, which in turn adversely affect comparisons made between measurements and predictions.

The measurements shown in Figure 3-2 were made at various temperatures, with the actual observation temperatures not reported. Instead, the measurements are presented by the various authors in graphical comparison with a theoretical curve at a "standard" or "normal" temperature, ranging from 288°K to 300°K. Compared to the absolute humidity, the measurement temperature is of considerably less importance in the variability of absorption due to water vapor. For this reason, all measurements of water vapor absorption, regardless of actual temperature, are plotted jointly in Figure 3-2.

Using the LIEBE and EOSAEL predictions at T=20°C as the reference predictions, one observes in Figure 3-2 that the majority of measurements within the 70-95 GHz frequency range verify best with the EOSAEL model prediction, with only measurements no. 3 and 5 in better agreement with the LIEBE prediction. Additionally, it is seen that the majority of these measurements are at or slightly below the EOSAEL model prediction. The large variability in measured vapor absorption is evident near 100 GHz, with two measurements in excess of the LIEBE model prediction and one below the EOSAEL model prediction. Above 100 GHz, seven of the nine observations are observed to be significantly in excess of the LIEBE model prediction; only measurement no. 18 verifies better with the EOSAEL model prediction than the LIEBE prediction. Overall, this "mixed" data set verifies better with the EOSAEL model at frequencies less than 100 GHz, and with the LIEBE model at frequencies greater than 100 GHz, with the agreement above 100 GHz not very satisfactory.

Other available experimental data sets for water vapor absorption are those described by Llewellyn-Jones and Knight (1981). They used an untuned resonant cavity equipped with precision temperature and humidity control to make laboratory measurements of water vapor absorption. Measurements by this team, at a frequency of 110 GHz and three different temperatures (273.7, 291.5, and 303.5°K), are shown in Figure 3-3. Overall, the measurements verify much better with the LIEBE model predictions than those of the EOSAEL model. This result certainly is not unexpected, since these experimental data of Llewellyn-Jones and Knight were used by Liebe (1983) in a comparison study with his model. Nonetheless, in spite of a probable bias toward the LIEBE model, the EOSAEL model prediction at T=291.5°K verifies better with absorption measurements with absolute humidities less than 5.5 g/m^3 than does the LIEBE prediction. In addition, at T=273.7°K, the agreement between these measurements with water content less than 2.5 g/m^3 and the EOSAEL model prediction appears about the same as the agreement between those measurements and the LIEBE model prediction. At each temperature, the departure of the EOSAEL model prediction from the measurements (and the LIEBE model prediction) increases as a function of absolute humidity.

3.1.3 Gaseous Absorption

LIEBE and EOSAEL model predictions of gaseous absorption, due to the combined effects of water vapor and molecular oxygen, are displayed in Figure 3-4 for a pressure of 1 atm., an absolute humidity of 7.5 g/m^3, and temperatures of 6.55, 20 and 30°C.

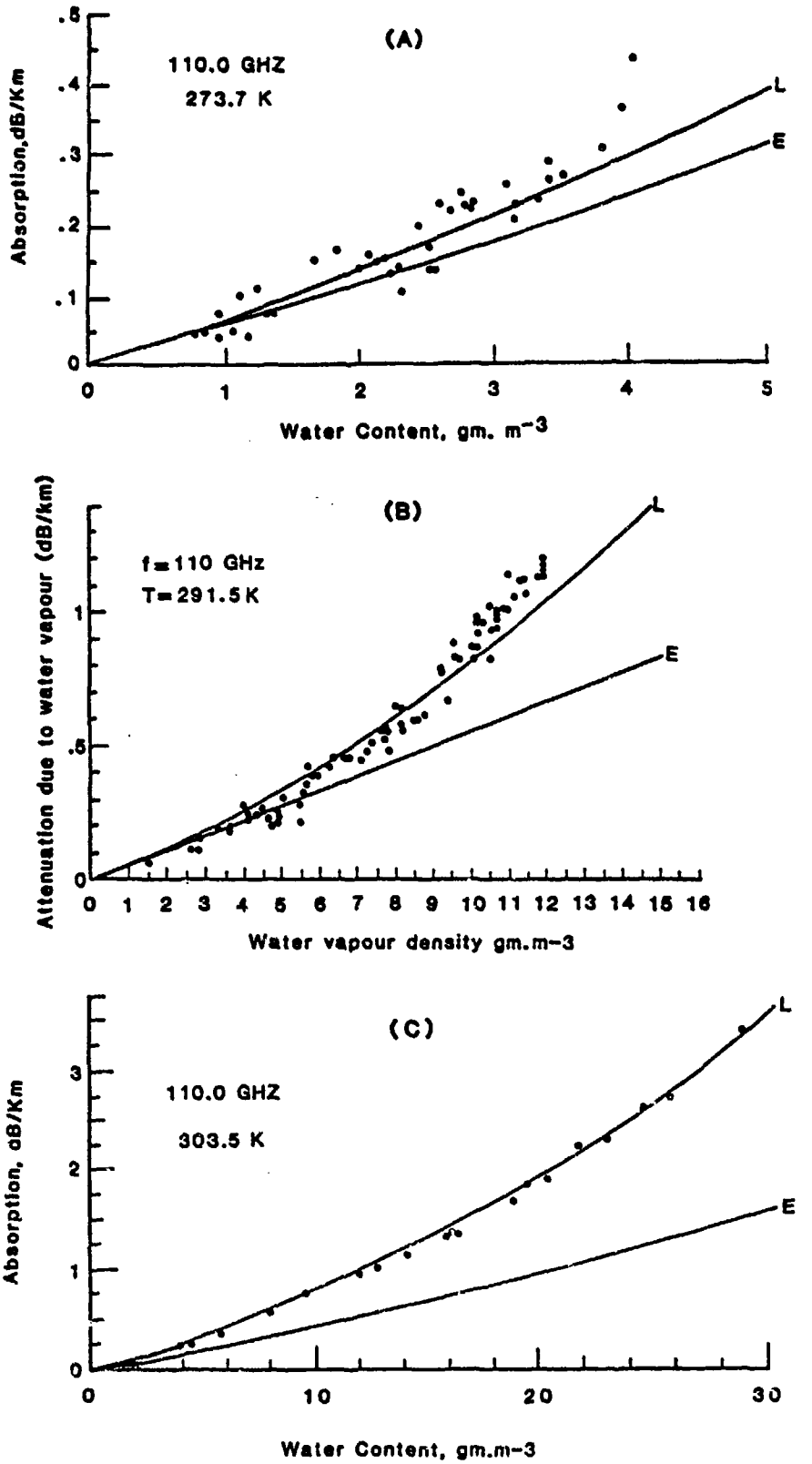

Figure 3-3. Comparison of LIEBE and EOSAEL Model Predictions of Water Vapor Absorption, with Laboratory Measurements at p=1 atm., F=110 GHz, and Three Temperatures: (a) 273.7°K, (c) 303.5°K (after Liebe (1983), after Knight and Llewellyn-Jones, 1982), and (b) 291.5°K (after Llewellyn-Jones and Knight, 1981).

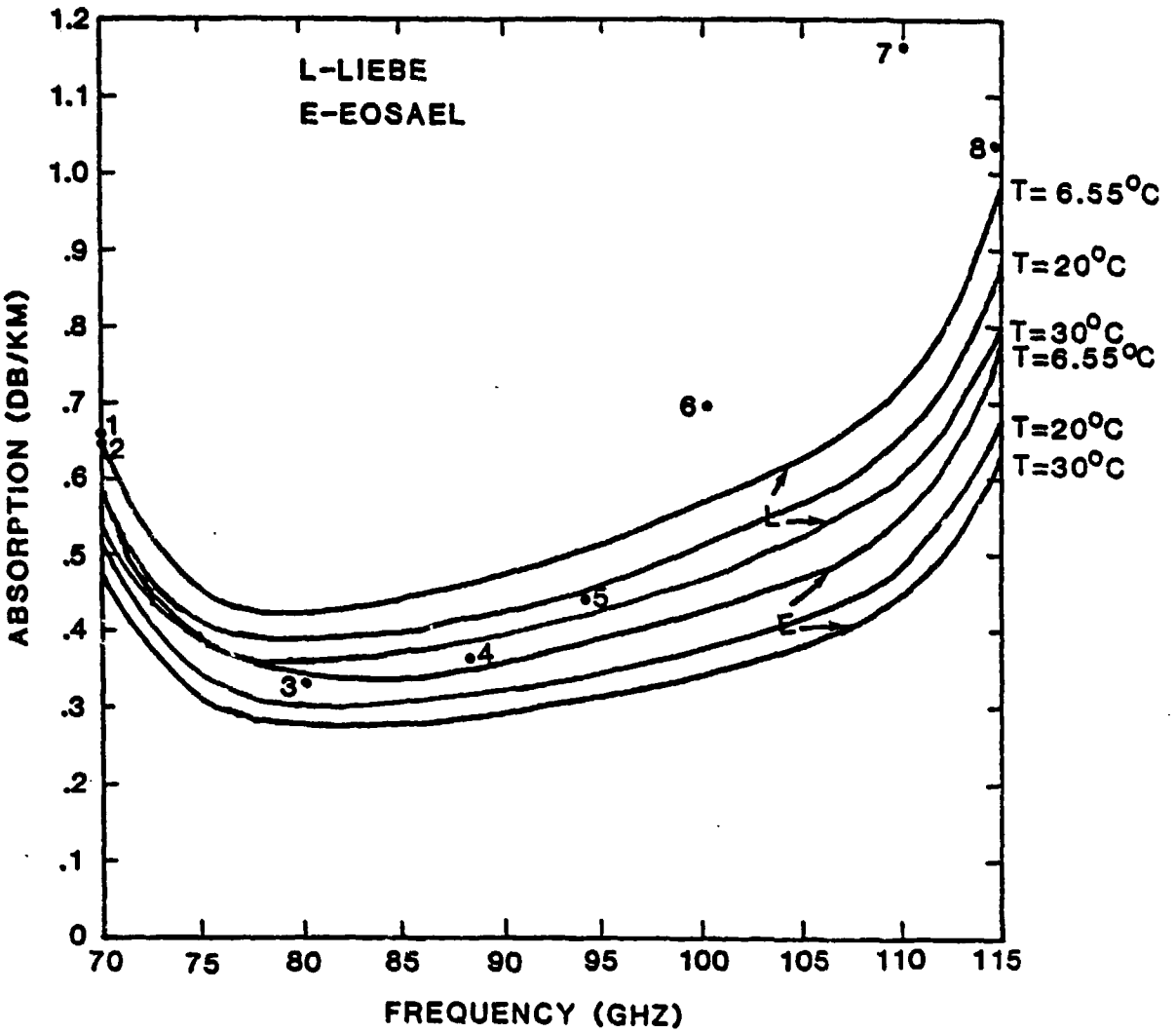

MEASUREMENT		
NO.	SOURCE	REFERENCE
1	University of Texas	Straiton and Tolbert (1960)
2	Bell Telephone Lab.	Hogg (1968)
3	Bell Telephone Lab.	Hogg (1968)
4	Bell Telephone Lab.	Hogg (1968)
5	Aerospace Corporation	Hoffman et al. (1966)
6	University of Texas	Straiton and Tolbert (1960)
7	University of Texas	Dryagin et al. (1966); Tolbert and Straiton (1961)
8	University of Texas	Hogg (1968)

Figure 3-4. Measured and Predicted Gaseous Absorption at $v=7.5\ g/m^3$, p=1 atm., F=[70,115] GHz, and T=[6.55,30]°C.

Eight field measurements, from three different sources, are also plotted. Analogous to the water vapor absorption measurements, these were taken at surface pressure and varying humidities and temperatures, and then adjusted to an absolute humidity of 7.5 g/m^3. Measurement number 5, the only one from the Aerospace Corporation, represents an average measurement of gaseous absorption during one summer month at El Centro, CA.

As can be seen in Figure 3-4, the LIEBE and EOSAEL models are in very good qualitative agreement. Both models predict a sharp decrease in gaseous absorption from 70 to 80 GHz, followed by a steady rise from 80 to 110 GHz, then a more abrupt increase from 110 to 115 GHz. A curve fit through the eight data points would verify this general behaviour of gaseous absorption as predicted by the LIEBE and EOSAEL models, although the curve fit to the data would show a much steeper increase of absorption with frequency over the 90-110 GHz frequency interval.

Overall, the measurements compare better with the LIEBE model prediction at T=20°C than with the EOSAEL model prediction for the same temperature. However, the two measurements which verify better with the EOSAEL model prediction (numbers 3 and 4) are both at frequencies near the theoretical minimum, which occurs between 80 and 85 GHz. The measurements at 100,110 and 114.8 GHz range from 60% to 150% in excess of the EOSAEL model prediction. Such large differences are hard to ascribe to experimental factors and errors, and suggest deficiencies in model prediction. These same measurements are also considerably in excess of the higher LIEBE model prediction.

Several other experimental data sets of gaseous absorption are available for model verification. Hogg (1980) measured absorption by atmospheric gases at 3.8 and 4.3mm (79 and 70 GHz) over a period of about one year in New Jersey by means of a reflection method. Figure 3-5a displays these measurements as a function of absolute humidity; linear and quadratic data fits are also plotted for both frequencies. No ambient temperatures are reported for the measurements. Figures 3-5b and c display the LIEBE and EOSAEL model predictions, respectively, superimposed on the data of Figure 3-5a. For these predictions, a pressure of 1 atm. and two different temperatures, 11.0°C and 22.55°C, were used. These temperatures were chosen for two reasons; one, they correspond to 100% relative humidities at 10 and 20 g/m^3 absolute humidities and, two, they closely correspond to the average annual and average summer temperature in New Jersey.

Overall, the EOSAEL model predictions verify better than the LIEBE model predictions at both 70 and 79 GHz. At 79 GHz, the EOSAEL model prediction at T=22.55°C compares very well with data and the linear and quadratic curve fits given by Hogg. At this same frequency, both LIEBE predictions exceed all measured values, with differences between predictions and measurements increased at higher absolute humidities. The model predictions of both LIEBE and EOSAEL at 70 GHz and T=11.0°C compare favorably with the measurements, although the absorption versus absolute humidity slope of the EOSAEL prediction is less steep and in

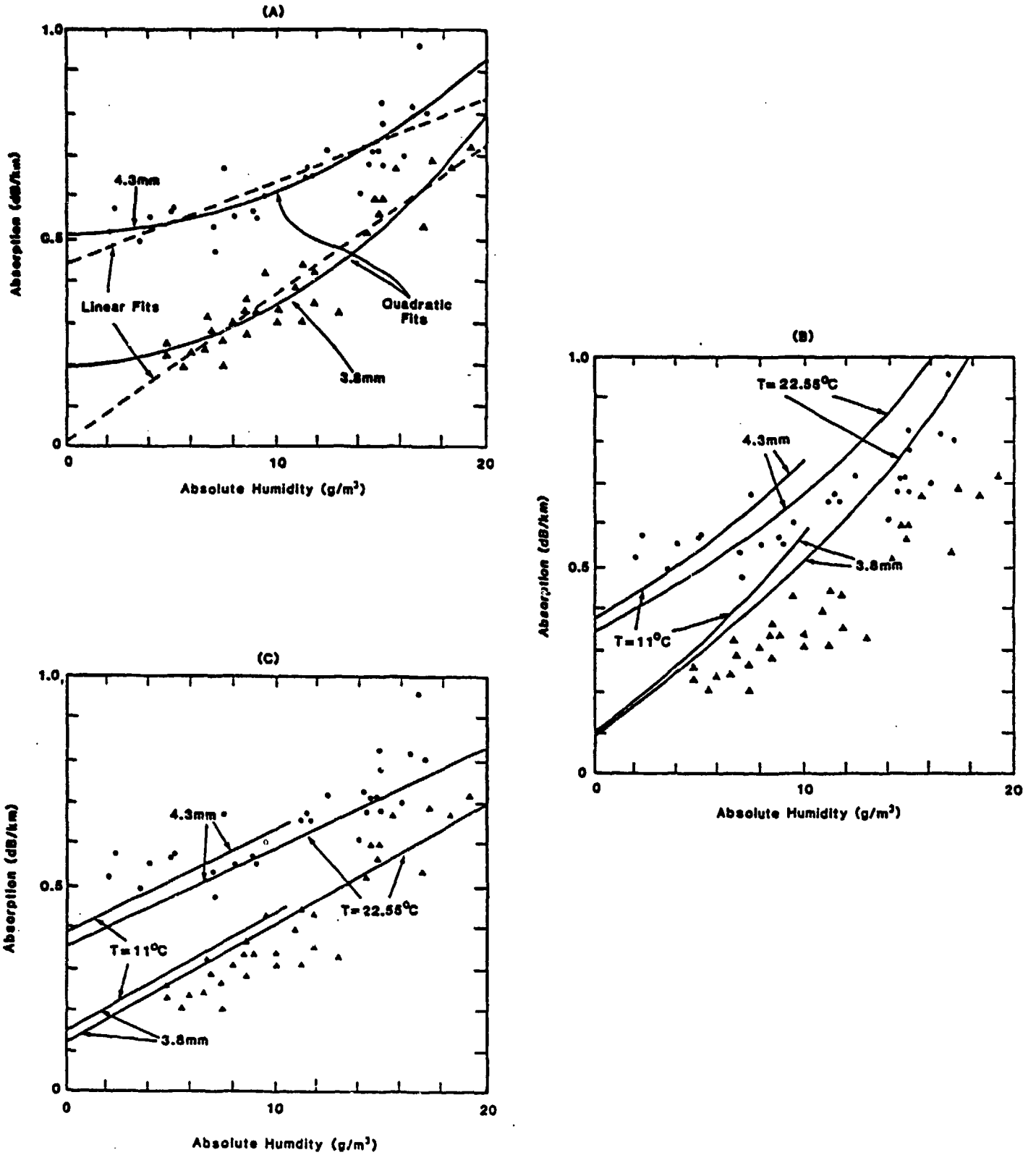

Figure 3-5. (a) Gaseous Attenuation at 3.8 mm (79 GHz) and 4.3 mm (70 GHz), for p=1 atm, and v=[0,20] g/m^3 (after Hogg, 1980). (b) Same as (a), with LIEBE Model Predictions at T=11^{o}C and T=22.55^{o}C. (c) Same as (a), with EOSAEL Model Predictions at T=11^{o}C and T=22.55^{o}C.

better agreement with the slope of the linear fit as given by Hogg. At high absolute humidities (>10 g/m^3), the LIEBE model prediction (with T=22.55°C) exceeds all measurements at 70 GHz, whereas the analogous EOSAEL prediction is in good agreement with both measurements and curve fits, albeit slightly low.

Another extensive experimental data set for gaseous absorption is that of Manabe et al. (1984). These measurements were made at a frequency of 81.84 GHz over a 0.81 km horizontal propagation path in Tokyo, Japan, during two periods of intensive observation - August 5-12, and Nov. 11-15, 1983. The representation of the data, as shown in Figure 3-6, is from Liebe (1985a). Here, the data points are actually clusters of original points condensed in dots in the course of a digitizing process. The two separate large groupings of data points of Figure 3-6 undoubtedly correspond to the separate periods of observation-fall for the 4-12 g/m^3 absolute humidity group, summer for the 16-22 g/m^3 absolute humidity group. Liebe (1985a) states that the gain stability of this experiment was estimated to be $\pm$0.3 db/km for attenuation over a temperature range of 0°C to 40°C. This suggests that the observed large scatter in data points is due to other factors besides signal instabilities.

For model comparison with observation, both the LIEBE and EOSAEL models were run at temperatures ranging from 0°C to 40°C. This range of temperature amply encloses the actual temperatures observed during the experiments. Overall, the LIEBE model predictions verify better with the measurements than the EOSAEL

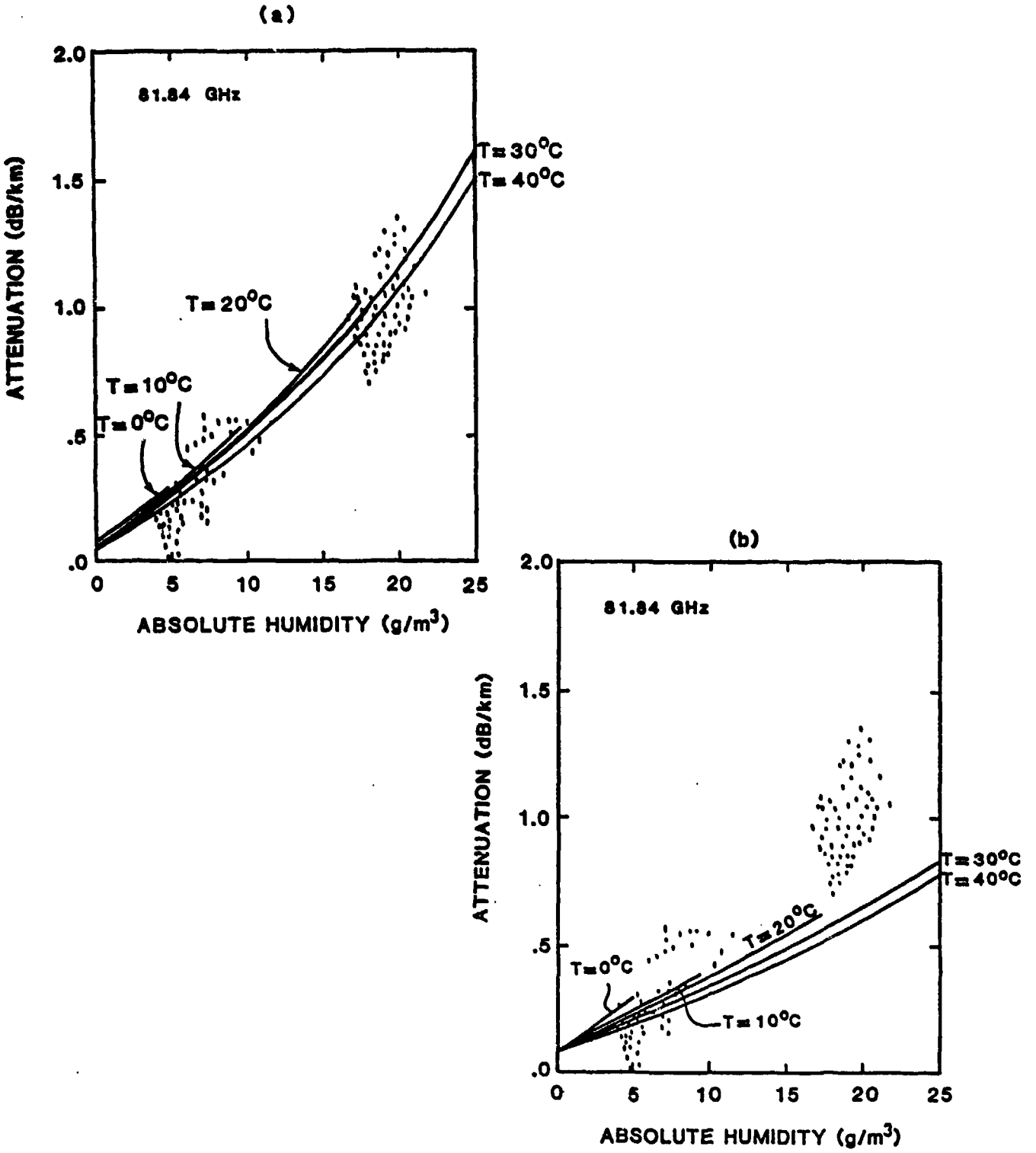

Figure 3-6. (a) Comparison of Liebe Model Predictions of Gaseous Absorption (at F=81.84 GHz, p=1 atm., and T=0,10,20,30,40 °C), with Measurements. Figure is after Liebe (1985a). Data Points are Representative of Measured Data of Manabe et al. (1984). (b) Same as (a), Except for EOSAEL Model Predictions.

predictions. This result is not unexpected since this data set was one of several used by Liebe (1985a,b) to lend credibility to his model. From Figure 3-6, it is observed that, whereas the LIEBE model predictions (with T=20-40^{o}C) are in good agreement with the "summer" measurements, the agreement between these observations and the EOSAEL predictions are not at all satisfactory, with all measurements being in excess of the predicted values. Below 12 g/m^3 absolute humidity, an accurate assessment of qualitative agreement between observations and predictions is not easy due to the large data scatter. The very low values of attenuation (<0.1 db/km) at absolute humidities near 5 g/m^3 do not seem reliable in that they are below the predicted value for absorption due solely to oxygen (given by the y-axis intercept). Even if one were not to consider these attenuation values <0.1 db/km near 5 g/m^3 absolute humidity, the remaining measurements near or at this absolute humidity would agree better with the EOSAEL model since, at all temperatures, its predicted values are slightly less than those of the LIEBE model. The many attenuation measurements near 0.5 db/km within the 6-12 g/m^3 absolute humidity range favor the LIEBE model prediction, although other data within this humidity range are quite low and agree better with the EOSAEL model prediction.

A final data set to be examined is that of Buijs and Janssen (1981). This team measured attenuation at 94 GHz over a .935 km propagation path near the seashore in The Netherlands, during a four month fall-winter period. The data, sampled at a rate of

1/hr at a temperature of 8±8°C, are represented in Figure 3-7 (after Liebe, 1985a), along with LIEBE and EOSAEL model predictions for temperatures of 0,8 and 16°C. For both attenuation as a function of absolute humidity and as a function of relative humidity, a large scatter in data points is evident. Those measurements observed to be well in excess of theoretical gaseous attenuation predictions, at absolute humidities of 4-8 g/m^3, are explained by hydrosol concentrations up to ~0.2 g/m^3 at relative humidities at or very near 100% (Liebe, 1985a).

In spite of the fact that this experimental data set was used by Liebe(1985a) to verify his model's predictive capability, the EOSAEL model predictions appear to agree better with the data. At T=8°C, the average temperature of the measurements, the LIEBE model prediction of attenuation as a function of absolute humidity exceeds the vast majority of the observations, whereas the EOSAEL prediction falls more closely toward the center of the dominant large data cluster. Even so, the EOSAEL prediction exceeds most measurements at absolute humidities <5 g/m^3. The LIEBE prediction at T=8°C of attenuation as a function of relative humidity is observed to exceed almost all values except those where haze transforms into fog (near 100% relative humidity). The analogous EOSAEL model prediction is in better agreement with the observations, although the EOSAEL model prediction at T=0°C provides the best fit to the observations.

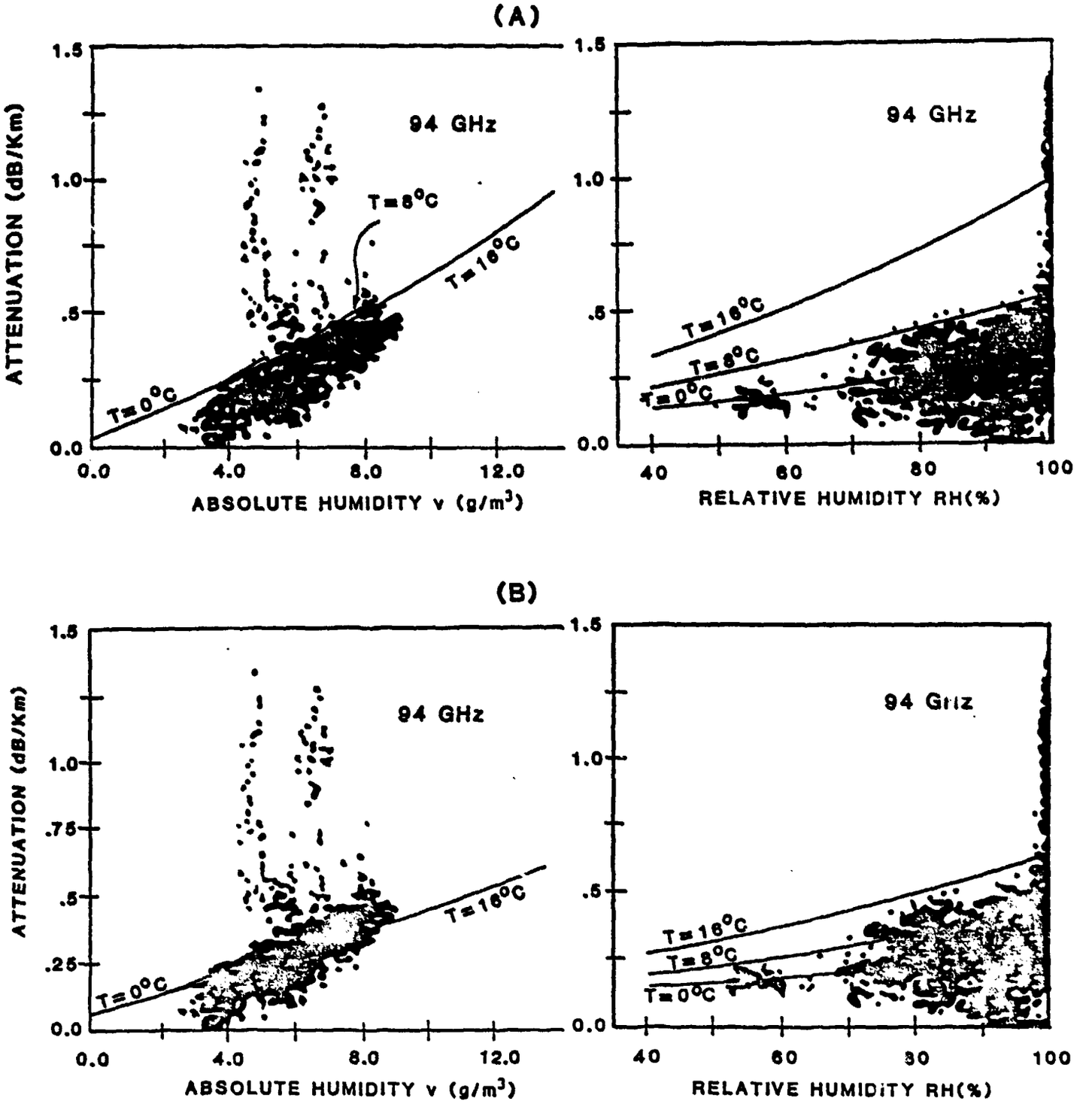

Figure 3-7. (a) Comparison of LIEBE Model Predictions of Gaseous Absorption (at F=94 GHz, p=1 atm., and T=0,8,16°C), with Measurements. Figure is after Liebe (1985a). Measured Data are at T=8°C, and are from Buijs and Janssen (1981). (b) Same as (a), Except for EOSAEL Model Predictions.

Taken collectively, the measurements presented in this subsection do not conclusively confirm superiority of either the LIEBE or EOSAEL model in the prediction of gaseous absorption. On the other hand, they do show that, qualitatively, both the LIEBE and EOSAEL model predictions of gaseous absorption are satisfactory.

3.2 Hydrometeor Effects

3.2.1 Fog Attenuation

Experimental fog attenuation data are scarce at millimeter wavelengths. The most extensive data are those reported by Richard et al. (1977), and shown in Figure 3-8. In this figure, measured fog attenuation by Richard et al. at 140 GHz and data from Robinson(1955) at 35 GHz are compared with theoretical calculations for radiation and advection fogs at these frequencies. The use of visibility to characterize fog, which allows measurements to be made with relative ease (as opposed to measurements of drop-size distribution or liquid water content), is less than ideal for purposes of correlation with millimeter wave attenuation since fogs of a specified liquid water content can vary greatly due to different droplet sizes. Specifically, advection fogs have a greater number of larger droplets (and thus greater visibilities) than radiation fogs. As a consequence, for a given visibility, an advective fog, with a larger liquid water content than a radiation fog, has a higher attenuation.

Without a suitable data set within the frequency range 70-115 GHz, the measured fog attenuation data of Robinson and Richard et al. at 35 and 140 GHz, respectively, can be used to

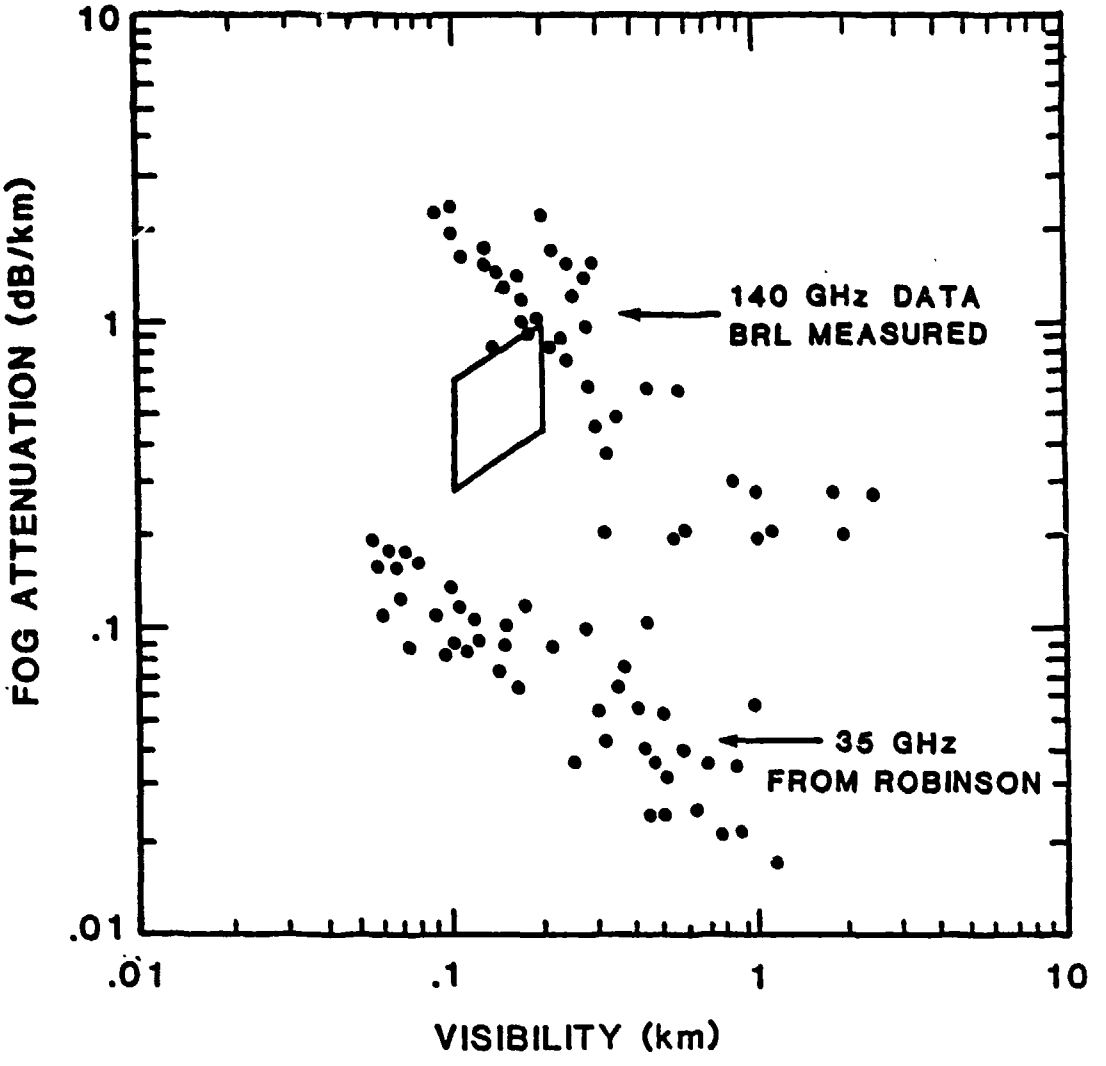

Figure 3-8. Measured Fog Attenuation at 35 and 140 GHz (after Richard et al., 1977). Measurements at 35 GHz are from Robinson (1955). Added Polygon Encloses LIEBE and EOSAEL Model Predictions at T=15°C, F=[70,115] GHz, and Visibility [100,200]m. For Model Calculations, Liquid Water Content Values w=[.11,.17] g/m^3 were Substituted for the Visibility Range [100,200]m.

verify, in a general way, the validity of the LIEBE and EOSAEL model predictions. This is possible since theory indicates that specific fog attenuation monotonically increases with frequency at millimeter wavelengths. The polygon shown in Figure 3-8 encloses the LIEBE and EOSAEL model predictions for fog attenuation at T=15°C, F=[70,115] GHz, and w=[.11,.17] g/m^3. The liquid water content limits were chosen to correspond to values reported by Koester and Kosowsky(1970) of typical fog characteristics; namely, w=0.11 g/m^3 and 100m visibility (for radiation fog), and w=0.17 g/m^3 and 200m visibility (for advection fog). With LIEBE model predictions exceeding EOSAEL model predictions, the lower side of the polygon corresponds to EOSAEL model predictions at F=70 GHz and w=[.11,.17] g/m^3, and the upper side of the polygon corresponds to LIEBE model predictions at F=115 GHz and w=[.11,.17] g/m^3. Based on the assumptions of decent measurements and a sound theory, the LIEBE and EOSAEL model predictions of fog attenuation at F=[70,115] GHz should lie between the measurements at 35 and 140 GHz. Figure 3-8 shows that this, indeed, is the case.

The only measurement of fog attenuation within the range 70-115 GHz to be found by this author is a report by Wrixon (1971) of an average attenuation due to heavy fog of 2.35 db at F=90 GHz and T=11°C. This measurement was made along an approximate 2.5 km path length through the atmosphere at a low zenith angle of about 23 degrees, using a sun tracker and receiver. At first view, this reported attenuation exceeds significantly that

predicted by either the LIEBE or EOSAEL model. An examination of the synoptic conditions at the observation time indicates the presence of frontal evaporative-type fog, which normally is characterized by fog at the surface and stratus with very light rain or drizzle aloft. Thus, if one assumes that the attenuation along the upper portion of the path length (~2 km) is due to drizzle (at α = 1 db/km), and the attenuation along the remaining 0.5 km portion of the path length nearest ground is due to fog (at α = 0.6 db/km), then the reported value for "fog" attenuation agrees reasonably well with either the LIEBE or EOSAEL model prediction.

3.2.2 Rain Attenuation

In this section, a comparison is made between the theoretical rainfall attenuation predictions of the LIEBE and EOSAEL models and observations from seven different sets of measurements found in the literature. As will be seen, the agreement between theory and observation is not completely satisfactory. This result should be expected if one considers the theoretical simplifications of the models in relation to the considerable experimental error due to, among others, the spatial inhomogeneity of rain, its strong variability in time, the difficulty in determining the applicable drop-size distribution and drop shape, the effects of wind and temperature, and the characteristics and limitations of rain collecting and drop-size measuring instruments.

All measurements used in model verification are displayed in Figures 3-9 through 3-20. In each figure, the LIEBE model prediction is labeled as "L". The three separate EOSAEL model predictions, based on the Marshall-Palmer, Joss drizzle, and Joss thunderstorm drop-size distributions, are labelled E(MP), E(D), and E(TS), respectively. The characteristics of individual data sets, and an assessment of their qualitative agreement with the LIEBE and EOSAEL model predictions, are now presented.

Usikov, German, and Vakser (1961)

The experimental data used for this report is that given by Medhurst (1965). The data was taken at λ=0.43 mm (70 GHz) by means of a reflection method over only a 50 m path length. Two rain gauges, separated by 30 m, were placed along the path. Attenuation readings were used only when rainfall intensities measured by the gauges were the same, and the intensity was not rapidly varying. Based on the experimental location (Russia), arbitrary rain temperatures of 10, 15 and 20^{o}C were assigned for the E(D), E(MP), and E(TS) model predictions, respectively. Figure 3-9 indicates that the measurements compare most favorably with the LIEBE model prediction though, on the average, the LIEBE model predictions exceed the measurements at rainrates greater than 10 mm/hr.

Hogg (1968)

Measurements were made by Bell Telephone Laboratories in New Jersey at a wavelength of 4.3 mm (70 GHz). Other specifics regarding the experimental setup are not readily available. Rain

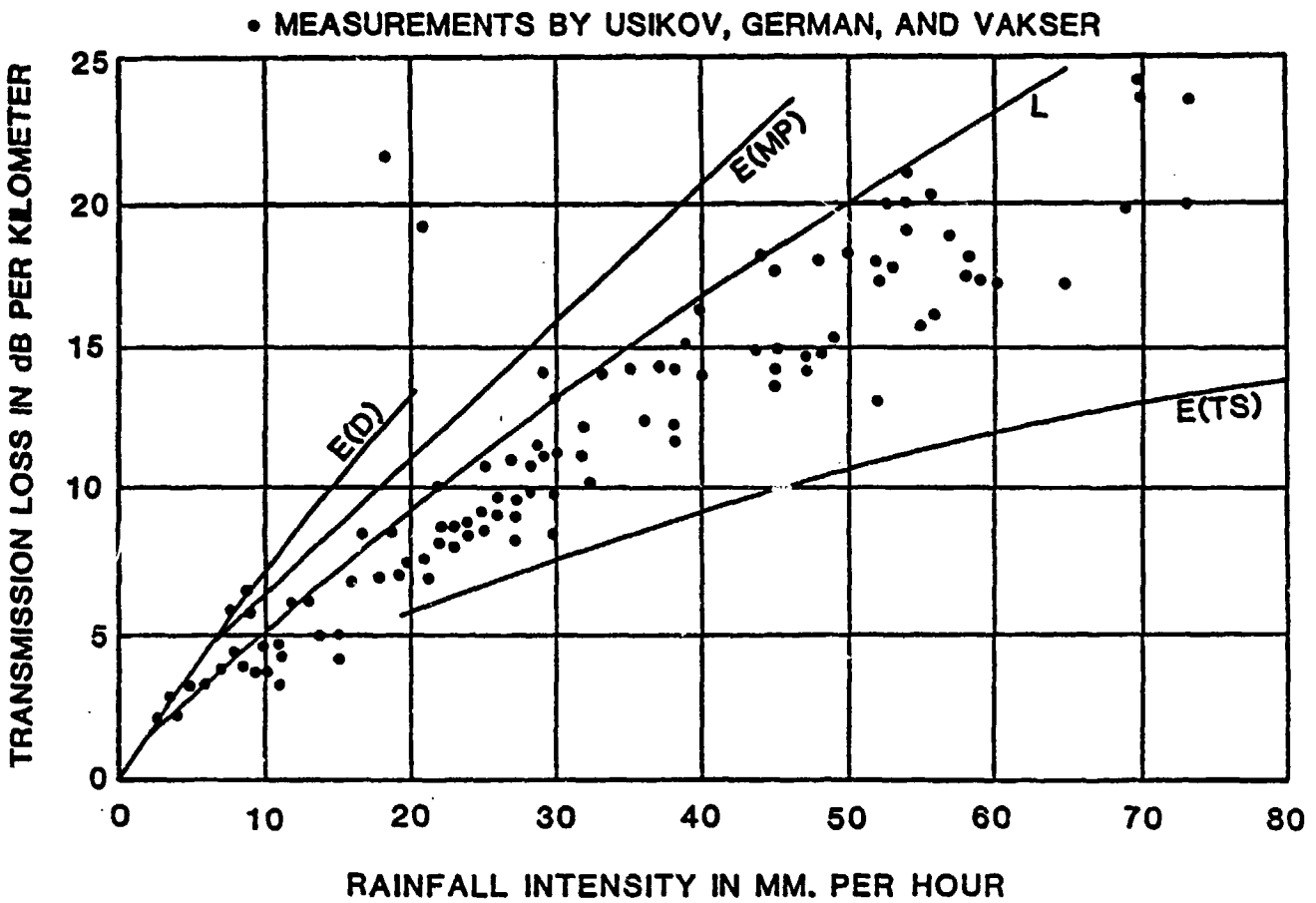

Figure 3-9. Measured Rainfall Attenuation, λ=0.43 cm (70 GHz) (after Medhurst (1965), after Usikov et al., 1961). Added Lines Indicate LIEBE and EOSAEL Model Predictions. Rain Temperatures of 10,15,20°C are Used for the E(D), E(MP), and E(TS) Model Predictions, Respectively.

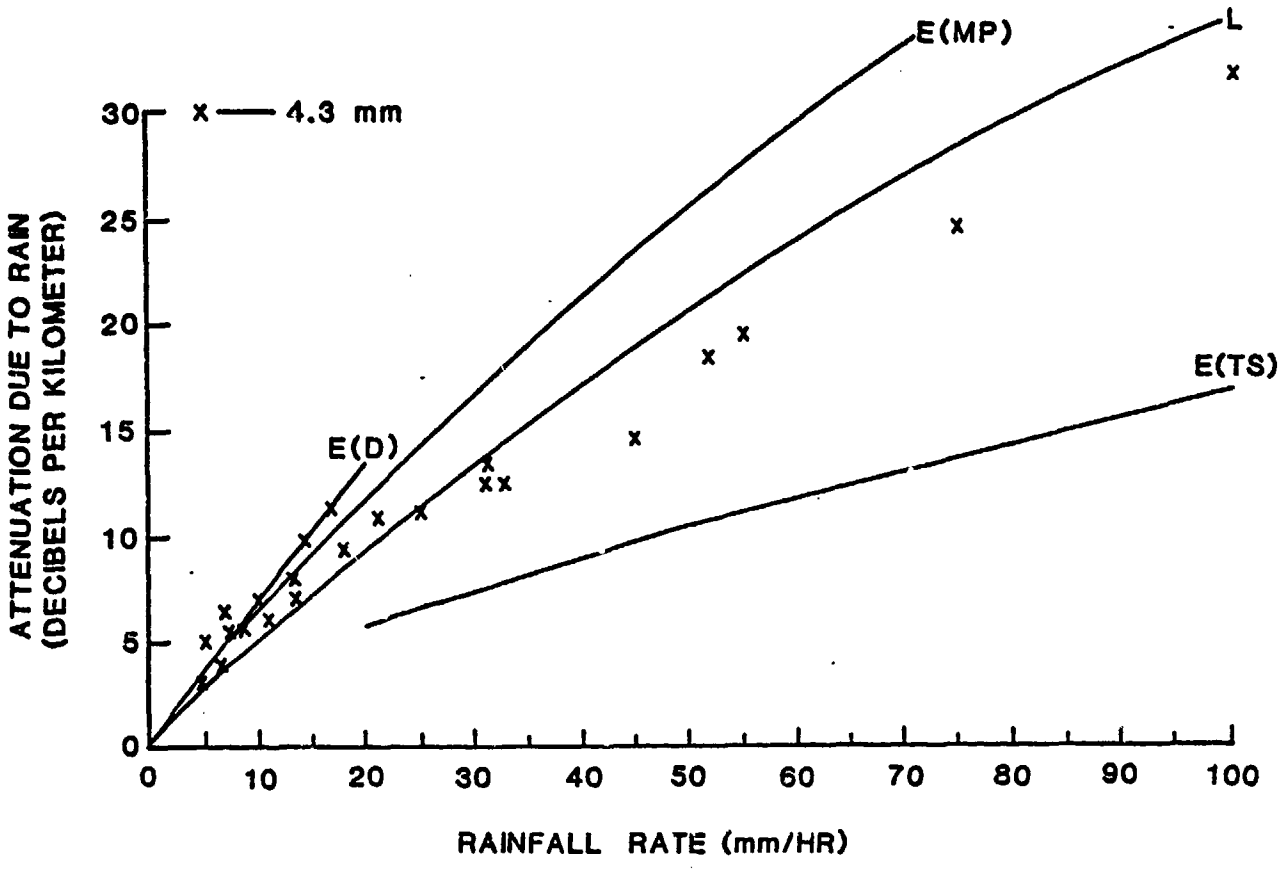

Figure 3-10. BTL Measurements of Attenuation due to Rain at 4.3 Millimeters (70 GHz) (after Hogg, 1968). An Added BTL Measurement at Rainfall Rate 100 mm/hr is from Hogg, 1969. Added Lines Indicate LIEBE and EOSAEL Model Predictions. Rain Temperatures of 10,15,20°C are used for the E(D), E(MP), and E(TS) Model Predictions, Respectively.

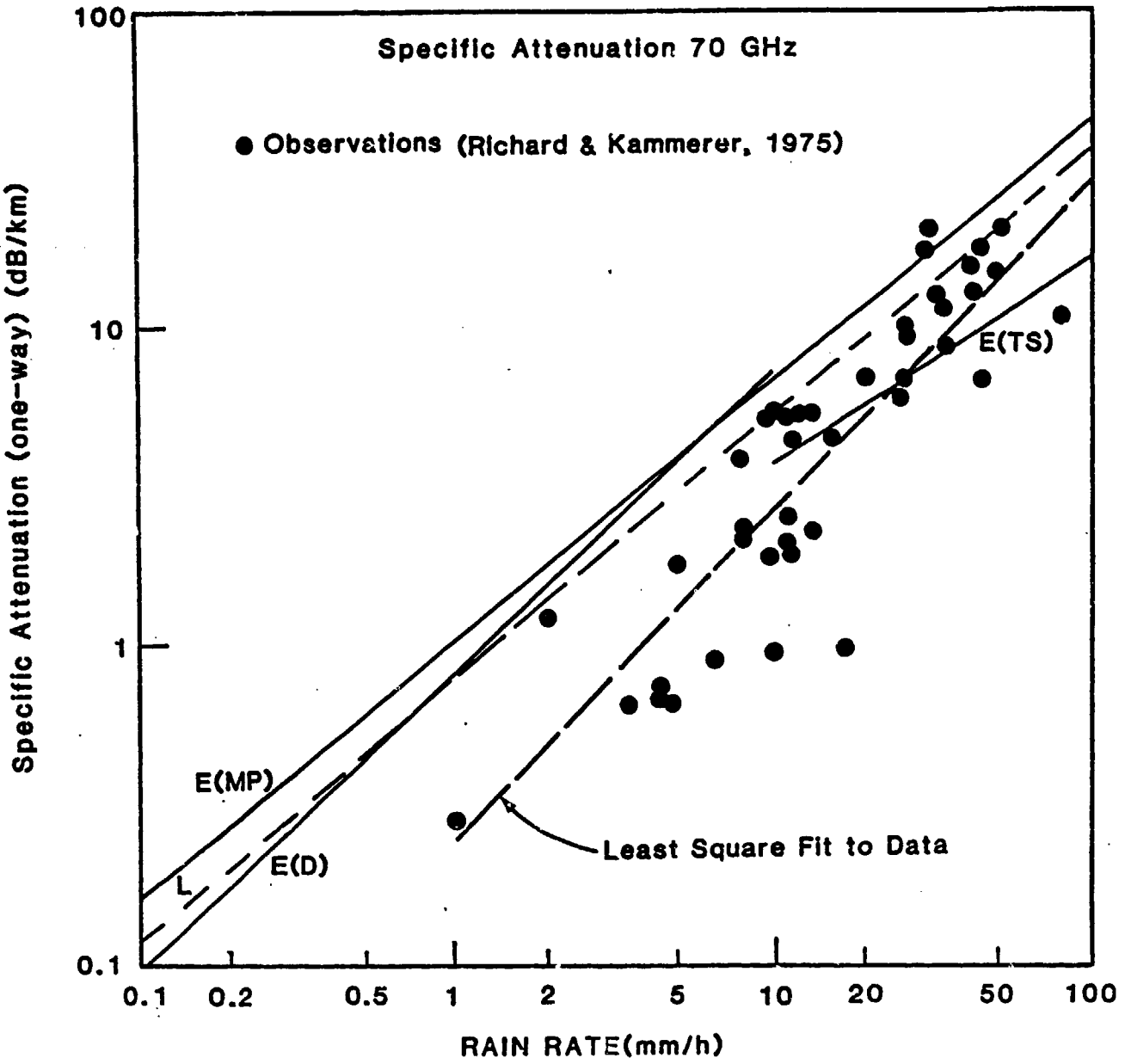

Figure 3-11. Specific Attenuation Observations at 70 GHz (after Crane and Burke (1978), after Richard and Kammerer, 1975). Added Lines Indicate LIEBE and EOSAEL Model Predictions. A Rain Temperature of 20°C is Used for All EOSAEL Model Predictions.

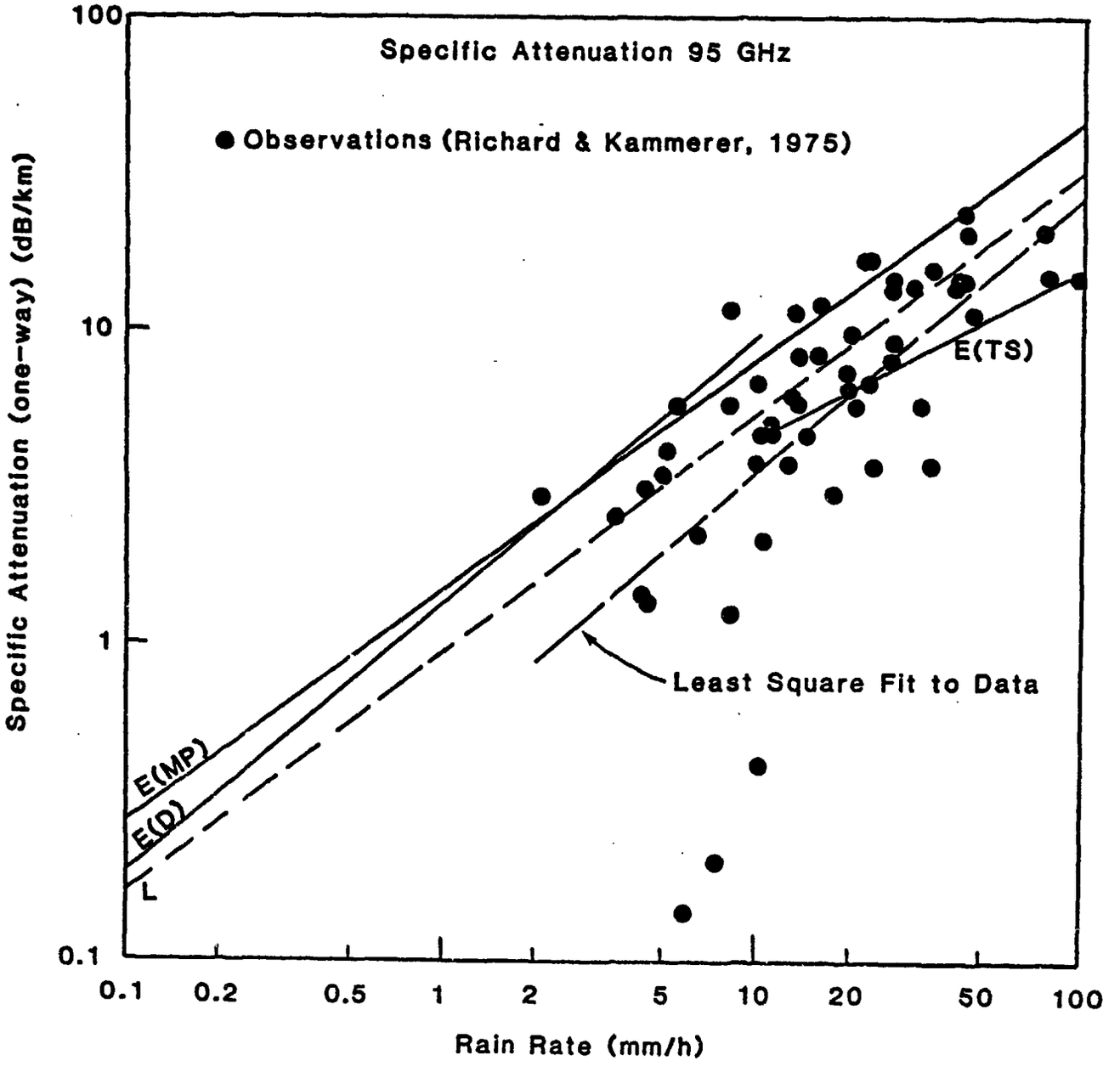

Figure 3-12. Same as Figure 3-11, Except at 95 GHz.

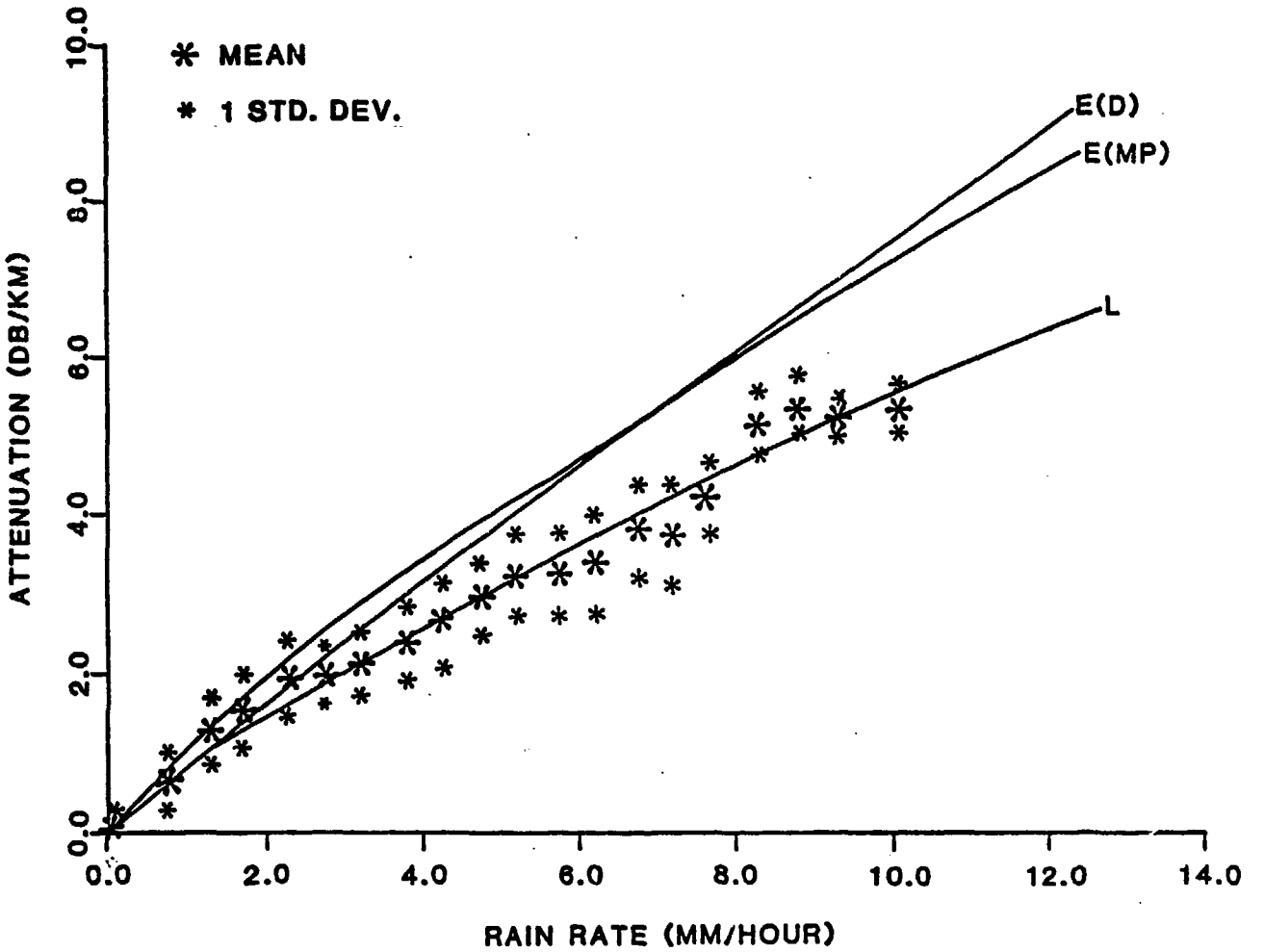

Figure 3-13. Mean Specific Attenuation Versus Path-Average Rain Rate (at F=74 GHz) for the Period 00:42 to 05:12h, February 12, 1977 (after Kharadly et al., 1978). Added Lines Indicate LIEBE and EOSAEL Model Predictions. A Rain Temperature of 10°C is Used for All EOSAEL Model Predictions.

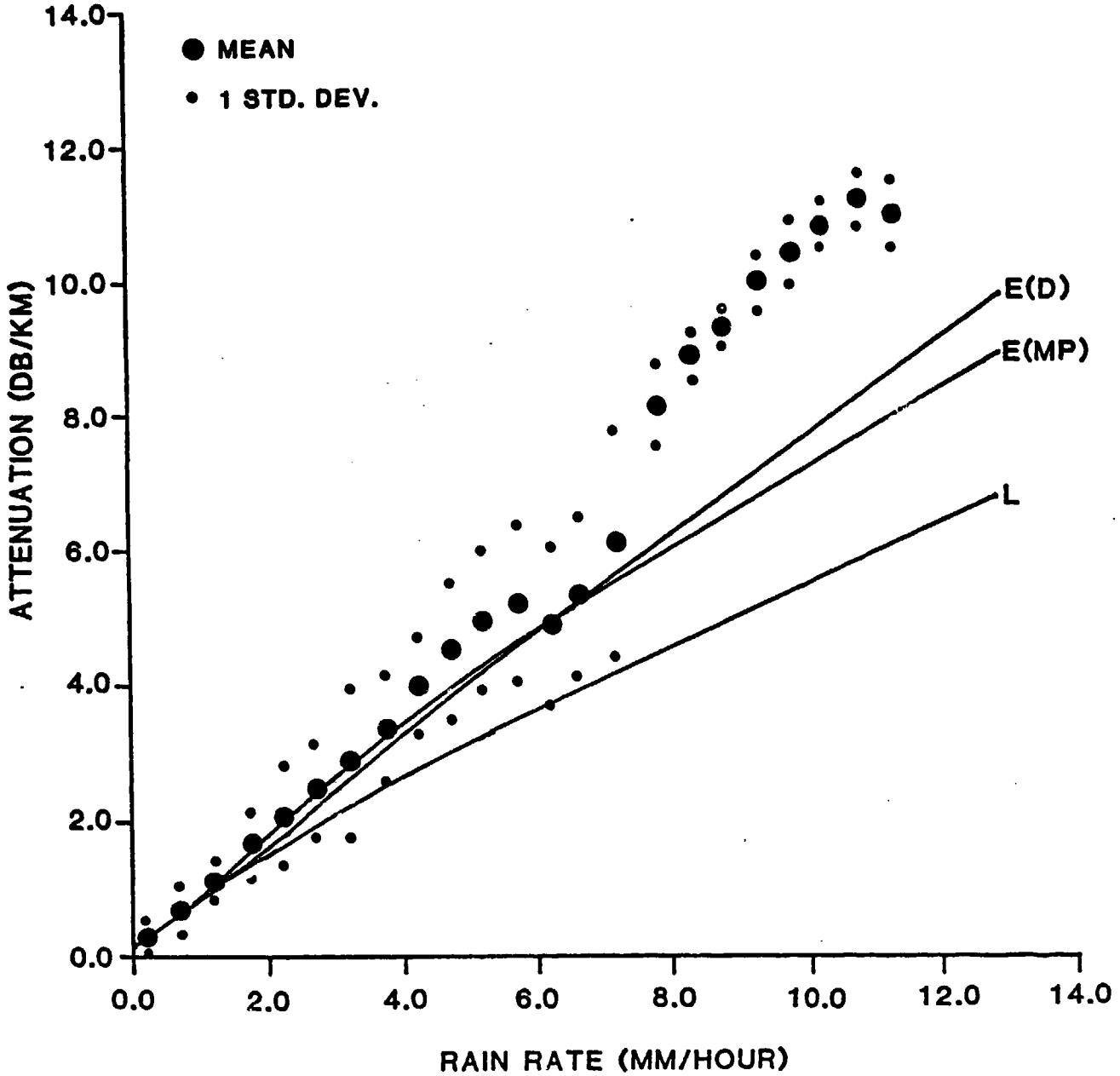

Figure 3-14. Same as Figure 3-13, Except for the Period 23:43h, May 30 to 22:43h, May 31, 1977.

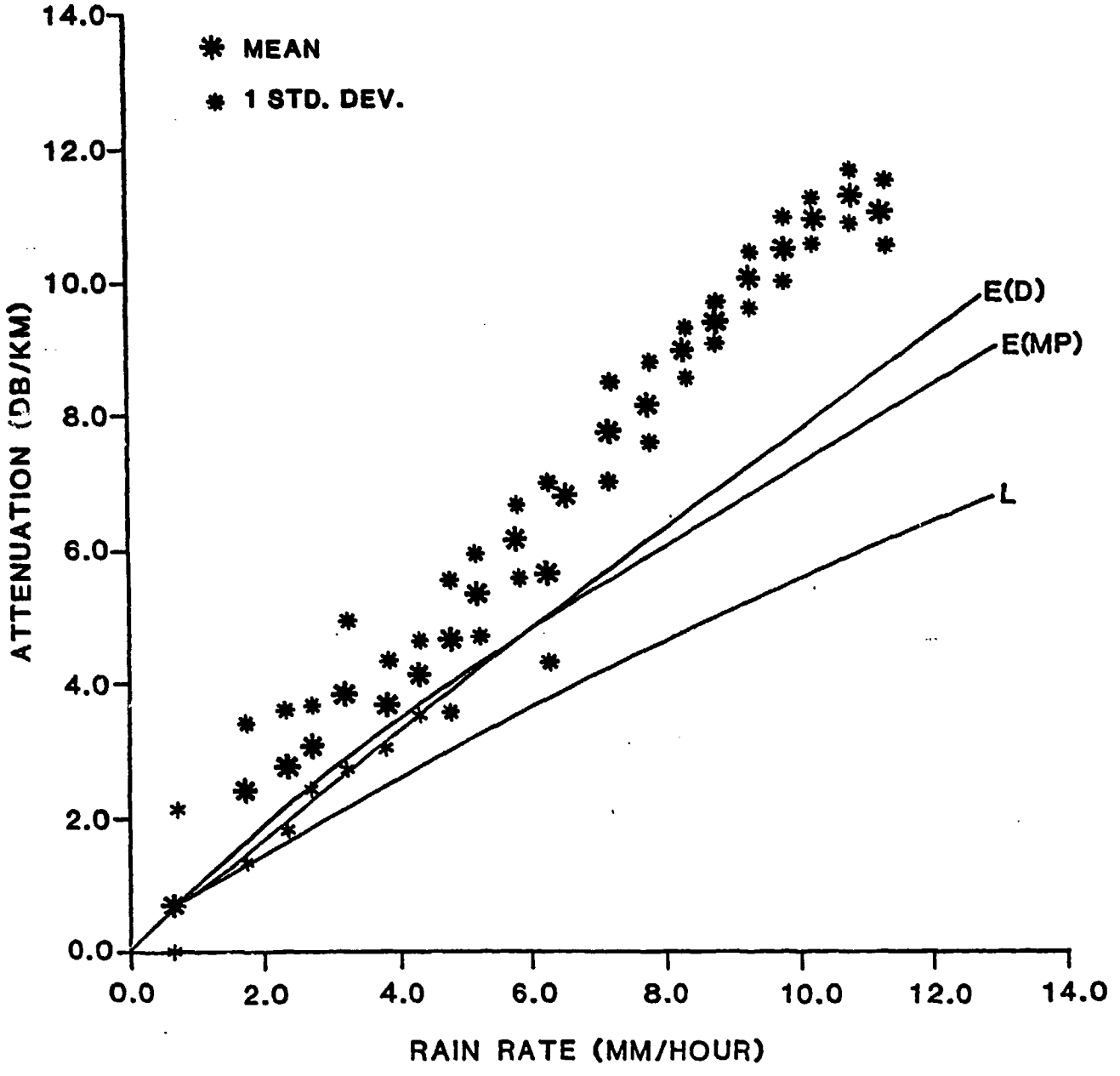

Figure 3-15. Same as Figure 3-13, Except for the Period 18:43 to 20:13h, May 31, 1977.

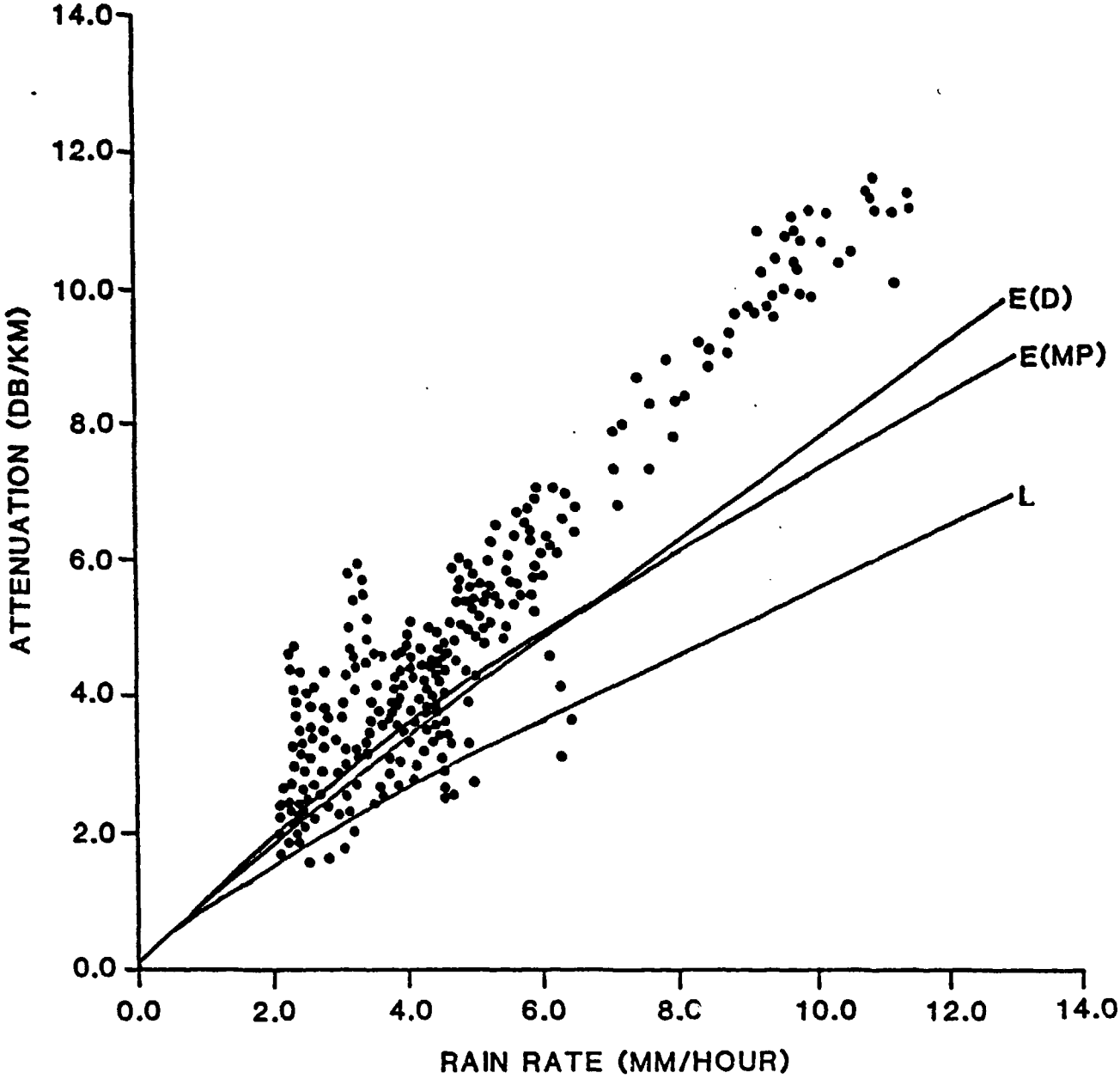

Figure 3-16. 10-Second Average Scatter Plot for the Period 18:43 to 20:13h, May 31, 1977 (after Kharadly et al., 1978). Added Lines Indicate LIEBE and EOSAEL Model Predictions at F=74 GHz. A Rain Temperature of 10°C is Used for All EOSAEL Model Predictions.

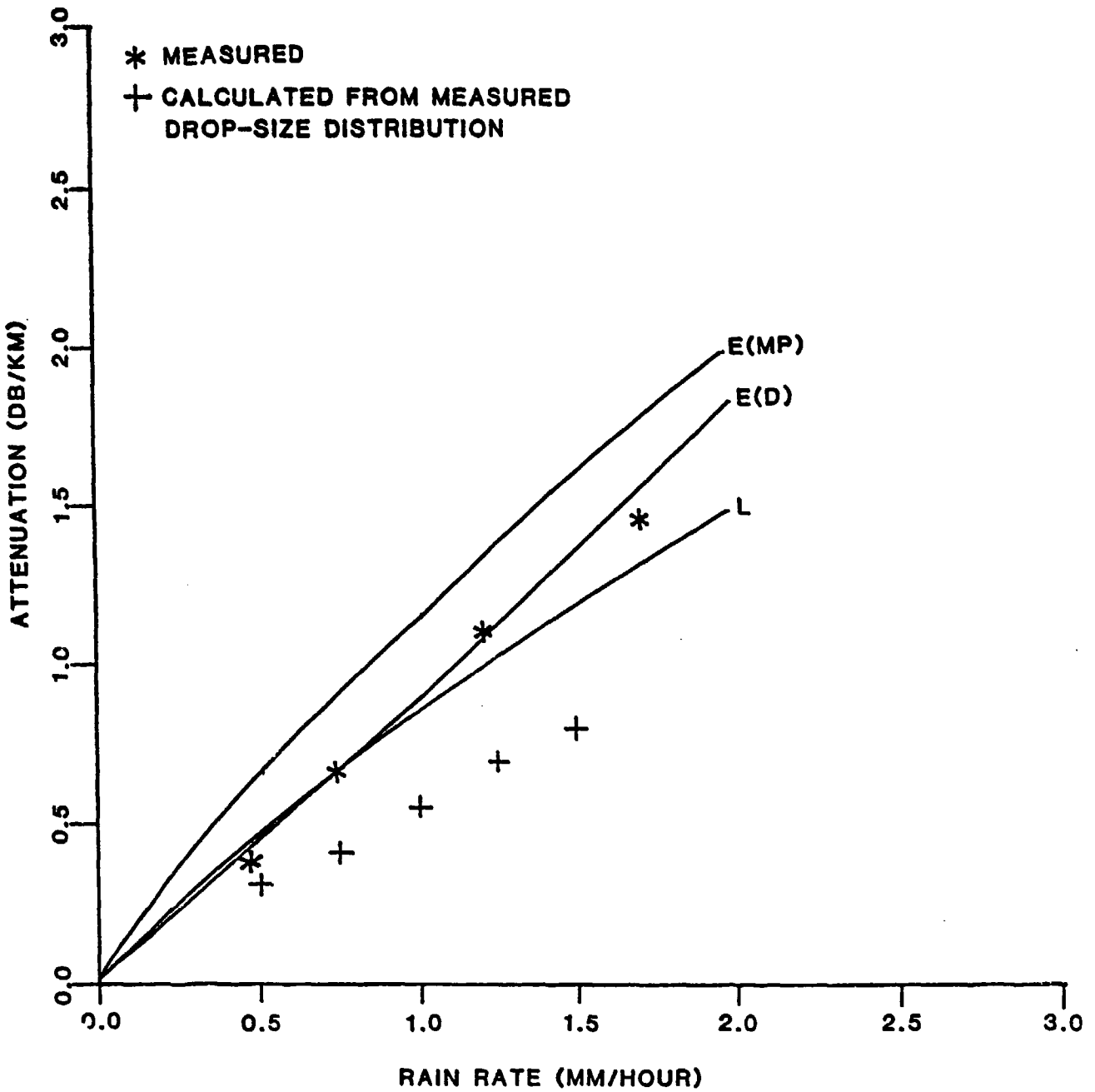

Figure 3-17. Comparison Between Measured and Calculated Values of Attenuation at 74 GHz for the Period 13:36 to 15:46h, May 26, 1978 (after Kharadly et al., 1978). Added Lines Indicate LIEBE and EOSAEL Model Predictions. A Rain Temperature of 10°C is Used for All EOSAEL Model Predictions.

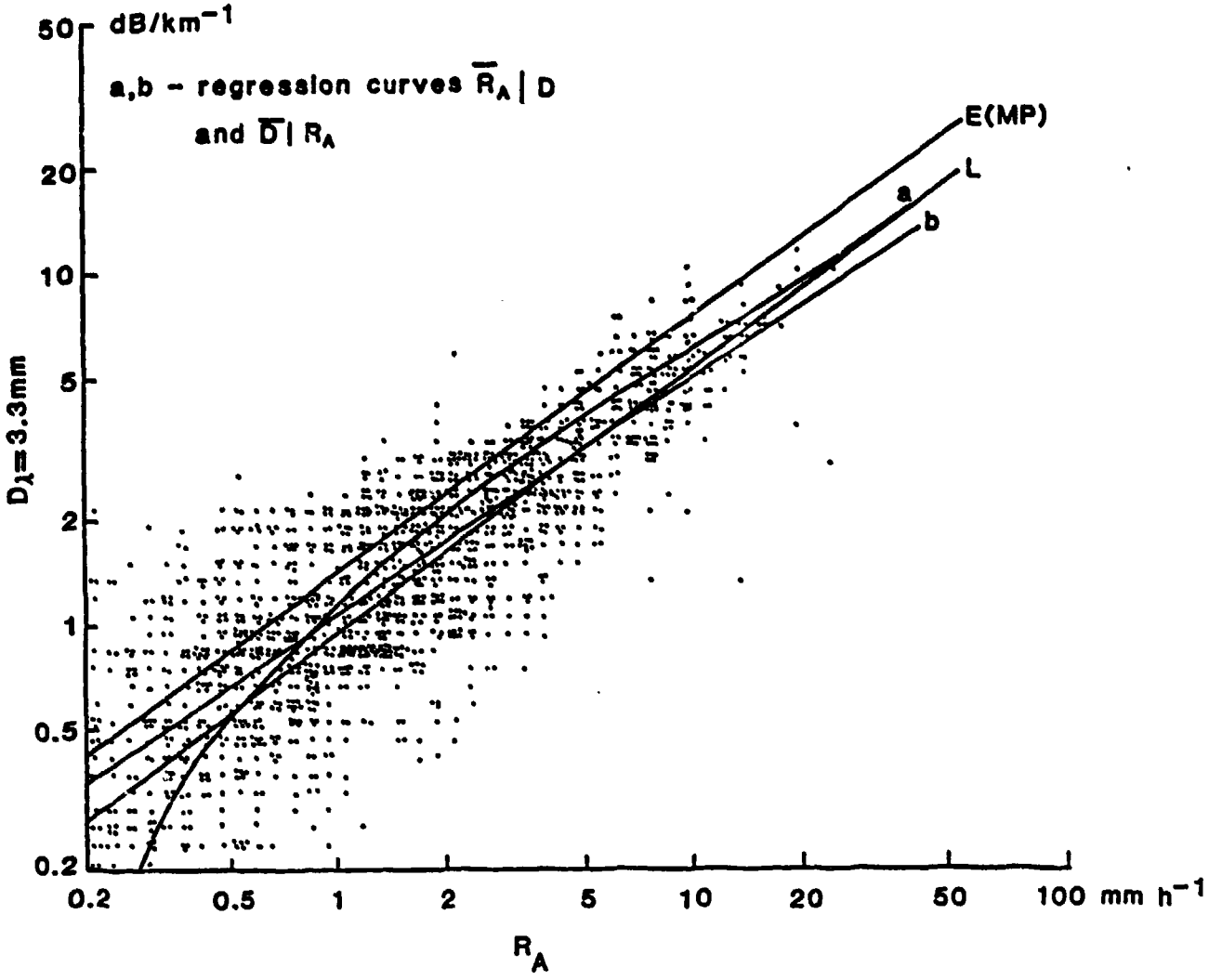

Figure 3-18. Measured Attenuation Coefficients Versus Rainfall Rate at λ=3.3 mm (90.8 GHz) (after Sander, 1975). Added Lines Indicate LIEBE and EOSAEL Model Predictions. A Rain Temperature of 10°C is Used for the EOSAEL Model Prediction.

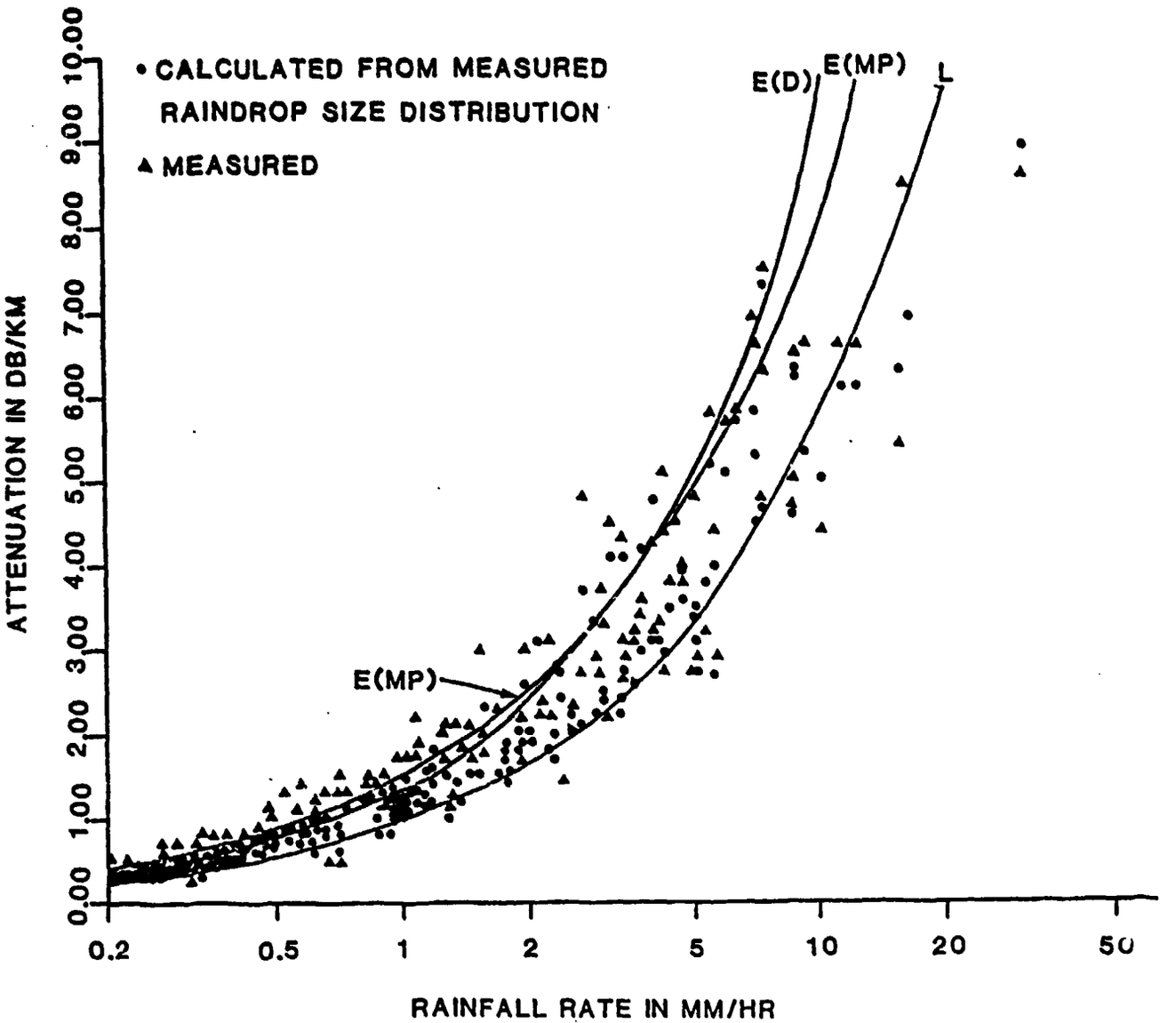

Figure 3-19. Measured and Calculated Attenuation Versus Rainfall Rate at 94 GHz (after Keizer et al., 1978). Added Lines Indicate LIEBE and EOSAEL Model Predictions. A Rain Temperature of 10°C is Used for All EOSAEL Model Predictions.

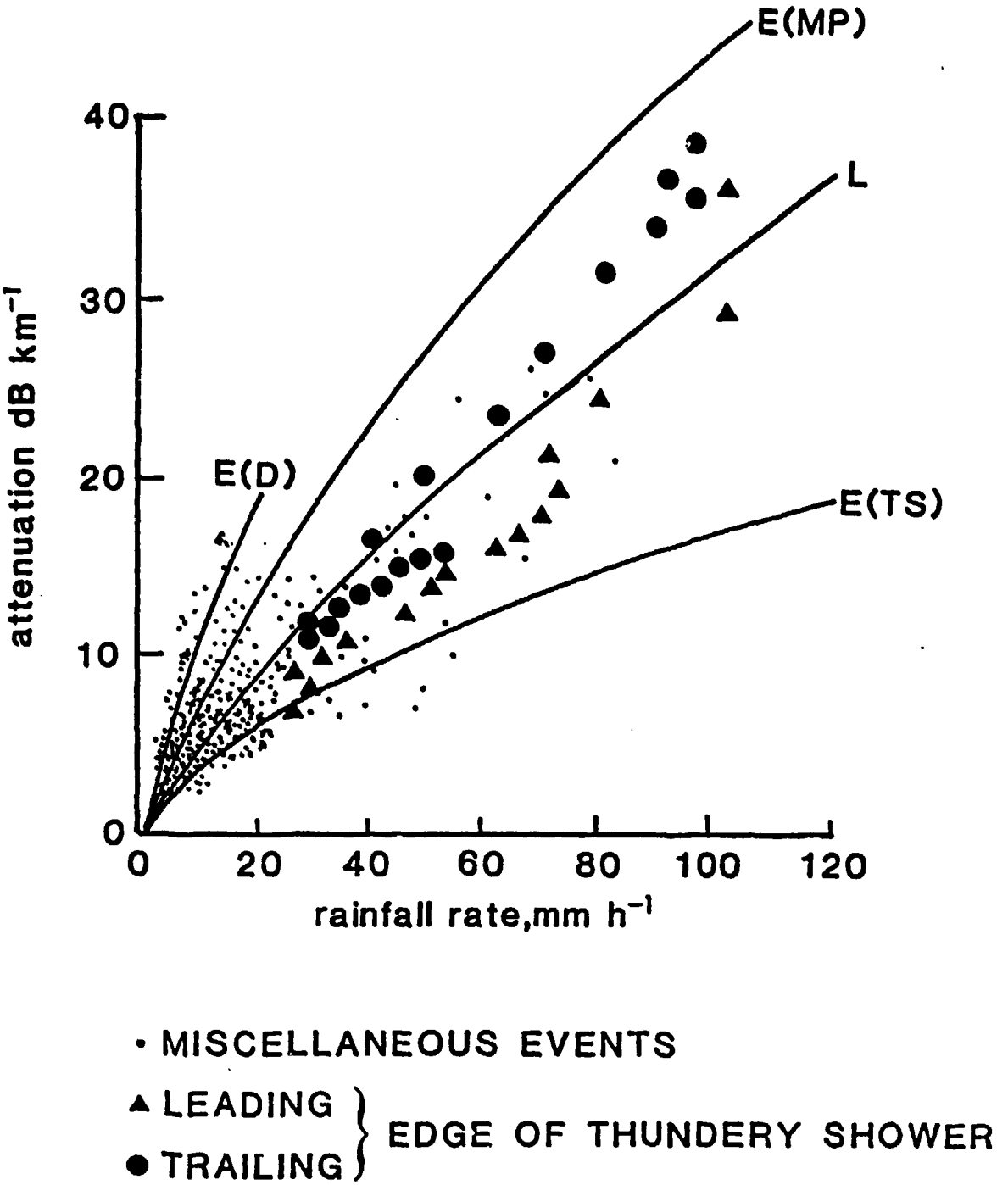

Figure 3-20. Variation of Attenuation with Rainfall at 110 GHz (after Zavody and Harden, 1976). Added Lines Indicate LIEBE and EOSAEL Model Predictions. A Rain Temperature of 15°C is Used for the E(D) and E(MP) Model Predictions, and a Temperature of T=20°C is Used for the E(TS) Model Prediction.

temperatures of 10,15, and 20°C were used for the E(D), E(MP), and E(TS) model predictions, respectively. As indicated by Figure 3-10, the LIEBE model prediction agrees best with measurements at rainrates greater than 20 mm/hr. At these moderate to heavy rainfall intensities, the E(TS) prediction is observed to fall well below all measurements. At lighter rainfall rates (less than 20 mm/hr), both the E(D) and E(MP) predictions appear to coincide better with the measurements than the LIEBE model prediction.

Richard and Kammerer (1975)

The observations used for this report, as given by Crane and Burke (1978), are radar measurements made in Florida by the Ballistics Research Laboratories of rain attenuation at 70 and 95 GHz. The data were obtained by comparing the cross section of a corner reflector observed during rain events with the cross section expected in the absence of rain. The rain was not measured along the 450 m path length but only at the target. This fact likely played an important role in the large scatter of observations at both 70 and 95 GHz (Figures 3-11 and 3-12, respectively).

This large scatter makes visual comparisons of observations with model predictions difficult although, in general, it can be seen that the LIEBE model predictions at both 70 and 95 GHz compare more favorably with the observations than either the E(MP) or E(D) predictions (with T=20°C). Nonetheless, the LIEBE model predictions are considerably above the least square power fits of Richard and Kammerer, especially at low rainfall rates.

The E(TS) predictions, also at T=20°C, appear to coincide better with certain observations than the LIEBE model predictions. However, at both frequencies, the attenuation versus rainrate slope for the E(TS) prediction agrees less with the slope of the least square fit than that for the LIEBE model prediction.

Kharadly, McNicol, and Peters (1978)

Measurements of rain attenuation at 74 GHz were obtained over an extended period of more than 100 hours at Vancouver, Canada. Five short-integration-time tipping-bucket rain gauges, spaced at 220 m intervals along a 0.9 km path length, were deployed to determine the path-average rain rate. Several examples of experimental results are shown in Figures 3-13 to 3-17, along with model predictions; for all EOSAEL model predictions, a rain temperature of 10°C is used.

For the four and a half hour wintertime rain storm of Figure 3-13, the LIEBE model prediction agrees very well with the mean specific attenuation at rainfall rates greater than 2.5 mm/hr, with the E(D) prediction being the most accurate at lower rain-rates. According to Kharadly et al., several other rainstorms yielded similar experimental results as those of this event.

The mean specific attenuation for an "off and on" 23 hour period of rain is depicted in Figure 3-14. The experimental results of this event are quite distinct from the proceeding example, and are reported by Kharadly et al. to be typical of other rain episodes. For this event, mean attenuation values are close to or exceed E(MP) and E(D) predictions for all

rainrates. Surprisingly, the observations exceed significantly the E(D) prediction at rainrates 8-12 mm/hr, even though this prediction can be considered as the upper bound for theoretical predictions.

To further examine this discrepancy between observations and and theoretical calculations, Kharadly et al. isolated a certain one and a half hour period during this extended rain event. As seen in Figure 3-15, the observed mean specific attenuation for this shorter time interval exceeds, at all rainrates, the maximum EOSAEL prediction (E(MP) for rainrates 0 to 6.2 mm/hr; E(D) for rainrates >6.2 mm/hr). A contributing factor for this discrepancy is believed to be the vertical wind (with peak values to 2 m/s) observed during this period, which would affect the instantaneous concentration of smaller drops in the transmission path and thus the attenuation. This idea is supported by Figure 3-16, which indicates a large observed variation in 10-sec average attenuation during this one and a half hour period at low rainrates, typical of drizzle or very light rain.

For this experiment, Kharadly et al. also measured drop-size distribution for a limited number of rain events using an electrostatic transducer. Figure 3-17 shows the comparison among measured attenuation, calculated attenuation from measured drop-size distribution, and several model predictions for a two hour rain episode. The E(D) model prediction is observed to fit very well with the measured attenuation during this very low

rainrate event, with the LIEBE model prediction also conforming well with the observations. The reasons for the discrepancy between the measured attenuation and that calculated from drop-size distribution are discussed by Kharadly et al.

Sander (1975)

A reflection method was used to measure rain attenuation at 90.8 GHz along a propagation path of total length 1008 m. Both standard integrating rain gauges and rain analyzers, at three points along the path, were used to determine rainfall rate. Figure 3-18 depicts 60-sec averages of attenuation (D) versus rainfall rate R_A, computed from the drop-size spectra as determined by the analyzers. Also depicted are the regression curves $\overline{R}_A|D$ and $\overline{D}|R_A$; the first regression valid under the assumption that R_A has been determined without error, the second, that errors in D are negligible. One notes that, in addition to the considerable scatter of data points, the LIEBE model prediction is in better agreement with the regression curves than the E(MP) model prediction (at $T=10^{o}C$).

Keizer, Snieder, and de Haan (1978)

Rain attenuation measurements at 94 GHz along a 935 m terrestrial path were made using a reflection method. Simultaneously, the raindrop size distribution was measured with an electromechanical distrometer, and the rainfall intensity recorded with three rapid-response rain gauges spaced about 500 m apart along the propagation path. Figure 3-19 displays measured attenuations (denoted by triangles) and calculated attenuations

based on measured drop-size distribution (denoted by dots) as functions of measured rainfall rate. Both measured attenuation and rainfall rate values are 83-sec averages. A rain temperature of 10°C is used for the depicted E(MP) and E(D) model predictions. At rainrates greater than 10 mm/hr, the LIEBE model is in best agreement with the measured and calculated attenuations. Within the intermediate rainfall intensity range (~2 to 10 mm/hr), no clear determination is possible, with all three predictions (L,E(MP), and E(D)) being in similar agreement with the measurements. At very low rainfall rates, the E(D) model prediction appears to agree slightly better qualitatively with the measured and calculated attenuation values than the LIEBE model prediction.

Zavody and Harden (1976)

Measurements of attenuation at 110 GHz on a path of 220 m were made during the summer,1974 at the Appleton Laboratory, England. Rainfall rates, averaged over 10-sec intervals, were recorded with four rapid-response rain gauges spaced about 40 m apart along the transmission path. For a few rain events, measured rain rates and attenuations were checked with information received on raindrop spectra from an analyzer, and found to be in reasonable agreement. Figure 3-20 displays experimental results and model predictions. A rain temperature of 15°C is used for the E(D) and E(MP) model predictions; a value of T=20°C is chosen for the E(TS) prediction. At very intense rain rates (90-100 mm/hr), all data points except one fall about halfway between the LIEBE and E(MP) predictions.

Overall, the LIEBE model prediction correlates best with measurements within the 20-90 mm/hr rainfall rate range. The majority of thundershower events within this range fall between the LIEBE and E(TS) predictions, with measured attenuations on the leading edge of thundershower events significantly lower than those reported on the trailing edge of such events. Zavody and Harden state that a reduction of drop sizes in a single shower is common and is confirmed by significant changes recorded in drop-size distributions. As expected, the EOSAEL model prediction based on the Joss thunderstorm distribution, with its dominance of larger drop sizes, agrees best with measured attenuations made on the leading edges of thundershowers. At low to moderate rainfall rates (<20 mm/hr), the comparison of model predictions with measurements is very difficult due to the large data scatter; as a result, no clear preference is indicated for either the LIEBE or E(MP) model prediction. Interestingly, there are many reported cases of high attenuation at low to moderate rainfall rates, a condition best predicted by the E(D) distribution, which contains a large number of small drops.

Seven Data Sets Collectively

Taken collectively, the seven experimental data sets indicate a better qualitative agreement with LIEBE model predictions than with EOSAEL model predictions at moderate to heavy rainfall rates (10-100 mm/hr). At very low rainfall rates (<2 mm/hr), typical of drizzle and very light rain, the E(D) prediction was in several cases in better agreement with observations than the LIEBE model prediction. In general,

the E(MP) predictions were most often found to be in excess of measured attenuation values, with the E(TS) attenuation predictions usually well below measurements at moderate to heavy rainfall intensities.

4. SUMMARY AND CONCLUSIONS

Two millimeter wave propagation models, the LIEBE and EOSAEL models, were evaluated for surface horizontal atmospheric attenuation within the frequency window 70-115 GHz. This evaluation involved intercomparisons of model theories and predictions, as well as comparisons of model predictions with measurements available from the literature. For model verification, one must be concerned with not only how close model predictions come to measurements but also how reliable are the measurements one uses for verification. The vast majority of the observations used for model comparison in this report are field observations, made under widely varying environmental conditions and prone to considerable experimental error. The LIEBE and EOSAEL mc predictions, based on simplifications to complicated theories, should be expected to differ from exact measurements. Based on the combination of these factors, actual measurements were found, in many cases, not to correspond too closely with the LIEBE and EOSAEL model predictions. A summary of findings, regarding the main sources of signal attenuation, is now presented.

Clear Atmosphere Effects

Molecular Oxygen - The theoretical bases of the LIEBE and EOSAEL models are essentially identical. Differences in model predictions are due to slightly varying parameterization values. Both models predict a decrease of O_2 absorption with temperature. Within the 70-115 GHz window, both models predict a minimum oxygen absorption near 100 GHz, of ~0.04 db/km at T=15°C. The few measurements available all exceeded theoretical calculations, especially those near the lower and upper bounds of the frequency window (70 and 115 GHz, respectively). This suggests that the theory of molecular O_2 absorption is not completely satisfactory.

Water Vapor - Theoretically, the LIEBE and EOSAEL models are substantially dissimilar in the calculation of water vapor absorption. In the EOSAEL model, absorption spectra are obtained by line-by-line calculations via a superkinetic line profile. Liebe employs a modified Van Vleck-Weisskopt function to calculate local line absorption as well as an empirical continuum spectra. LIEBE model predictions at typical meteorological conditions indicate that the continuum absortion is the dominant contributor to the total water vapor absorption. Although both the LIEBE and EOSAEL models predict an increase of absorption with frequency, model predictions can be in substantial disagreement, especially at high absolute humidities.

The temperature dependence of the absorption slope is found to differ substantially in the models at high values of relative humidity. While laboratory data sets at 110 GHz show good agreement with the LIEBE model and rather poor agreement with the EOSAEL model (except at low water vapor densities), field measurements from diverse sources suggest that both LIEBE and EOSAEL model predictions are too low at frequencies 100 to 115 GHz. Both models compare more favorably with those field observations within the 70-100 GHz frequency range.

Under normal operating conditions, devoid of adverse weather, gaseous absorption (O_2+ H_2O vapor absorption) is the principal limiting effect on surface millimeter wave propagation; as such, its reliable prediction is of prime importance. Qualitatively, LIEBE and EOSAEL model predictions of gaseous absorption are in agreement within the 70-115 GHz frequency window, although, at a high absolute humidity, the LIEBE model prediction is significantly in excess of that of EOSAEL. Interesting, both measurements and theoretical predictions indicate that the minimum for gaseous attenuation within the 70-115 GHz window is not at 94 GHz but at a lower frequency. Both the LIEBE and EOSAEL models predict this minimum near 90 GHz at T=0^{o}C, decreasing to near 80 GHz at T=30^{o}C. In spite of the large data scatter common to several experimental data sets, comparisons between measurements and

both models are in qualitative agreement. The measurements, however, do not conclusively indicate a superiority of either the LIEBE or EOSAEL model in gaseous attenuation prediction.

Hydrometeors

Fog - The LIEBE and EOSAEL models both use the Rayleigh approximation of Mie scattering theory in the prediction of fog attenuation. Slight differences in model predictions can be ascribed to selection of parameterization values. Attenuation due to fog is forecast by both models to increase with frequency and liquid water content, and decrease with temperature. Although observations for the 70-115 GHz frequency range were generally unavailable, fog attenuation measurements at 35 and 140 GHz were used to verify that predictions by both the LIEBE and EOSAEL models were in reasonable agreement with theory.

Rain - Due to the cumbersomeness of the full Mie scattering calculations, both the LIEBE and EOSAEL models use a simplistic empirical power law relation between attenuation and rainfall rate. This procedure requires the assumption of a dropsize distribution, which for the LIEBE model is the Laws Parsons distribution. The EOSAEL model allows the user the option of three dropsize distributions: the Marshall-Palmer (for widespread rain), and the Joss drizzle and thunderstorm. At all rainfall rates, attenuation predictions of the EOSAEL model, using the MP dropsize distribution, are in excess of the LIEBE model predictions,

with differences larger at higher frequencies. Overall, various experimental data sets show a better agreement with the LIEBE model prediction. At very low rainfall rates, the EOSAEL model prediction based on the Joss drizzle distribution is observed to be in very good agreement with the measurements of several data sets.

Due to theoretical simplifications and considerable experimental error, an accurate and definitive assessment of model performance is quite difficult. Results presented in this report indicate that, while the qualitative agreement between either the LIEBE or EOSAEL model predictions, and measurements, for horizontal attenuation due to oxygen, water vapor, fog and rain is certainly satisfactory, there is still a definite need for improvement.

The preference of either the LIEBE or EOSAEL model over the other for operational use is certainly not clear-cut. Data comparisons suggest that, for several attenuation types, model preference is dependent on either the frequency or meteorological conditions.

Due to the highly modular structure of the LIEBE and EOSAEL models, the transfer of singular features from one model to the other would not be difficult. Such features include the EOSAEL model's capabilities for input of absolute humidity values for gaseous attenuation calculations, rain attenuation calculations based on the JOSS drizzle dropsize distribution, and snow attenuation prediction; and the LIEBE model's capabilities for calculation of zenith attenuation and refractive dispersion.

REFERENCES

Bastin, J.A., 1966: Extreme Infra-Red Atmospheric Absorption, Infrared Physics, Vol. 6, pp 209-221.

Brown, D.R., 1984: Near Millimeter Wave Module NMMW, EOSAEL 84, Vol. 6, Rep. ASL-TR-0160-6, USAERCDC Atmos. Sci. Lab., White Sands Missile Range,N.M.

Buijs, J.H., and L.H. Jannsen, 1981: Comparison of Simultaneous Atmospheric Attenuation Measurements at Visible Light, Infrared (3-5 μm) and MM-waves (94 GHz), Physics Lab., NDRD, The Netherlands, Report No. PHL 1981-04, January.

Chang, A.T., and T.T. Wilheit, 1979: Remote Sensing of Atmospheric Water Vapor, Liquid Water, and Wind Speed at the Ocean Surface by Passive Microwave Techniques from the NIMBUS 5 Satellite, Radio Science, Vol. 14, No. 5, pp 793-802.

Crane, R.K., and H.K. Burke, 1978: The Evaluation of Models for Atmospheric Attenuation and Backscatter Characteristic Estimation at 95 GHz, ERT Document No. P-3606, Environmental Research and Technology, Inc., Concord, MA., Feb.

Dryagin, Yu. A., A.G. Kislyakov, L.M. Kukin, A.I. Naumov, and L.I. Fedoseev, 1966: Measurement of the Atmospheric Absorption of Radio Waves in the Range 1.36-3.0 mm, Izvestiya VUZ. Radiofizika, Vol. 9, No. 6, pp 624-627.

Gibbins, C.J., A.C. Gordon-Smith, and D.L. Croom, 1975: Atmospheric Emission Measurements at 85 to 118 GHz, Planet. Space Sci., Vol. 23, pp 61-73.

Hoffman, L.A., H.J. Wintroub, and W.A. Garber, 1966: Propagation Observations at 3.2 Millimeters, Proc. of the IEEE, Vol. 54, No. 4, pp 449-454.

Hogg, D.C., 1968: Millimeter-Wave Communication Through the Atmosphere, Science, Vol. 159, No. 3810, pp 39-46.

Hogg, D.C., 1969: Statistics on Attenuation of Microwaves by Intense Rain, Bell System Technical Journal, Vol. 48, pp 2949-2963.

Hogg, D.C., 1980: "Ground-based Measurements of Microwave Absorption by Tropospheric Water Vapor," in Atmospheric Water Vapor, eds. A. Deepak, T.D. Wilkerson, and L.H. Ruhnke, New York, Academic Press, pp 219-228.

Keizer, W.P.M.N., J. Snieder, and C.D. de Haan, 1979: Rain Attenuation Measurements at 94 GHz: Comparison of Theory and Experiment, NATO AGARD Conference Proceedings No. 245, Feb.

Kharadly, M.M., J.D. McNicol, and J.B. Peters, 1979: Measurement of Attenuation Due to Rain at 74 GHz, NATO AGARD Conference Proceedings No. 245, February.

Knight, R.J., and D.T. Llewellyn-Jones, 1982: Measurements of Water Vapour Absorption in the RAL untuned cavity, Rutherford Appleton Lab. Research Note RL-82-051, July.

Koester, K.L., and L.H. Kosowsky, 1970: "Attenuation of Millimeter Waves in Fog," Amer. Meteorol. Soc., 14th Radar Meteorol. Conference, Tucson, Az., pp 231-236.

Liebe, H.J., G.G. Gimmestad, and J.D. Hopponen, 1977: Atmospheric Oxygen Microwave Spectra-Experiment Versus Theory, IEEE Trans. Antennas and Propagation, Vol. AP-25, No. 3, pp 327-335.

Liebe, H.J., 1980: "Atmospheric Water Vapor: A Nemesis for Millimeter Wave Propagation," in Atmospheric Water Vapor, eds. A. Deepak, T.D. Wilkerson, and L.H. Ruhnke, New York, Academic Press, pp 143-201.

Liebe, H.J., 1983: An Atmospheric Millimeter Wave Propagation Model, NTIA Rep. 83-137, Natl. Telecommun. and Inform. Admin., Boulder,CO., Dec.

Liebe, H.J., 1985a: Millimeter-Wave Propagation in Moist Air: Model Versus Path Data, NTIA Rep. 85-171, Natl. Telecommun. and Inform. Admin., Boulder,CO.,March.

Liebe, H.J., 1985b: An Updated Model for Millimeter Wave Propagation in Moist Air, Radio Science, Vol. 20, No. 5, pp 1069-1089.

Llewellyn-Jones, D.T., and R.J. Knight, 1981: Molecular Absorption by Atmospheric Gases in the 100-1000 GHz Region, IEE Conf. Publ. 195 (ICAP 81), pp 81-83.

Manabe, T., Y. Furuhama, T. Ihara, S. Saito, H. Tanaka, and A. Ono, 1984: Measurements of Attenuation and Refractive Dispersion due to Atmospheric Water Vapor at 80 and 240 GHz, Conf. Digest, 9th Intl. Conf. on Infared and Millimeter Waves, Takarazuka, Japan F-3-3, pp 465-466.

Medhurst, R.G., 1965: Rainfall Attenuation of Centimeter Waves: Comparison of Theory and Measurement, IEEE Trans. Antennas and Propagation, Vol. AP-26, pp 550-564.

Olsen, R.L., D.V. Rodgers, and D.B. Hodge, 1978: The aR^b Relation in the Calculation of Rain Attenuation, IEEE Trans. Antennas and Propagation, Vol. AP-26, No. 2, pp 318-329.

Ray, P.S., 1972: Broadband Complex Refractive Indices of Ice and Water, Applied Optics, Vol. 11, No. 8, pp 1836-1844.

Richard, V.W., and J.E. Kammerer, 1975: Rain Backscatter Measurements and Theory at Millimeter Waves, BRL Report 1838, USA Ballistics Research Laboratories, Aberdeen Proving Ground, Md.

Richard, V.W., J.E. Kammerer, and R.G. Reitz, 1977: 140 GHz Attenuation and Optical Visibility Measurements of Fog, Rain, and Snow, U.S. Army Ballistic Research Laboratories Memorandum Report, ARBRL-MR-2800, December.

Robinson, N.P., 1955: Measurements of the Effect of Rain, Snow, and Fogs on 8.6 mm Radar Echoes, Proc. of the IEE, Vol. 203B, pp 709-714.

Sander, J., 1975: Rain Attenuation of Millimeter Waves at λ= 5.77,3.3, and 2 mm, IEEE Trans. Antennas Propagation, Vol. AP-23, No. 2, pp 213-220.

Schulze, A.E., and C.W. Tolbert, 1963: Shape, Intensity and Pressure Broadening of the 2.53-Millimeter Wave-Length Oxygen Absorption Line, Nature, Vol. 200, No. 4908, pp 747-750.

Straiton, A.W., and C.W. Tolbert, 1960: Anomalies in the Absorption of Radio Waves by Atmospheric Gases, Proc. of the IRE, Vol. 48, No. 5, pp 898-903.

Tolbert, C.W., and A.W. Straiton, 1961: An Analysis of Recent Measurements of the Atmospheric Absorption of Millimetric Radio Waves, Proc. of the IRE, Vol. 49, No. 2, pp 649-650.

Usikov, O. Ya., V.L. German, and I. Kh. Vakser, 1961: Investigation of the Absorption and Scatter of Millimeter Waves in Precipitations, Ukr. Fiz. Zh., Vol. 6, pp 540-618.

Wrixon, G.T., 1971: Measurements of Atmospheric Attenuation on an Earth-Space Path at 90 GHz Using a Sun Tracker, Bell System Technical Journal, pp 103-114.

Zavody, A.M., and B.N. Harden, 1978: Attenuation/Rain-rate Relationships at 36 and 110 GHz, Electronic Letters, Vol. 12, No. 17, pp 422-424.

DISTRIBUTION

ASST. FOR ENV. SCIENCES
ASST. SEC. OF THE NAVY (R&D)
ROOM 5E731, THE PENTAGON
WASHINGTON, DC 20350

CHIEF OF NAVAL RESEARCH (2)
LIBRARY SERVICES, CODE 784
BALLSTON TOWER #1
800 QUINCY ST.
ARLINGTON, VA 22217-5000

OFFICE OF NAVAL RESEARCH
CODE 1122AT, ATMOS. SCIENCES
ARLINGTON, VA 22217-5000

OFFICE OF NAVAL RESEARCH
ENV. SCI. PROGRAM, CODE 112
ARLINGTON, VA 22217-5000

OFFICE OF NAVAL TECHNOLOGY
ONR (CODE 22)
800 N. QUINCY ST.
ARLINGTON, VA 22217-5000

CHIEF OF NAVAL OPERATIONS
(OP-096)
U.S. NAVAL OBSERVATORY
WASHINGTON, DC 20390

CHIEF OF NAVAL OPERATIONS
OP-962
U.S. NAVAL OBSERVATORY
WASHINGTON, DC 20390

DIRECTOR
NATIONAL SECURITY AGENCY
ATTN: LIBRARY (2C029)
FT. MEADE, MD 20755

OJCS/J3/ESD
THE PENTAGON, ROOM 2B887
WASHINGTON, DC 20301-5000

COMNAVOCEANCOM
ATTN: CODE N5
NSTL, MS 39529-5000

COMMANDING OFFICER
NAVAL OCEANOGRAPHIC OFFICE
BAY ST. LOUIS
NSTL, MS 39522-5001

COMMANDING OFFICER
FLENUMOCEANCEN
MONTEREY, CA 93943-5005

SUPERINTENDENT
LIBRARY REPORTS
U.S. NAVAL ACADEMY
ANNAPOLIS, MD 21402

DIRECTOR OF RESEARCH
U.S. NAVAL ACADEMY
ANNAPOLIS, MD 21402

NAVAL POSTGRADUATE SCHOOL
METEOROLOGY DEPT.
MONTEREY, CA 93943-5000

NAVAL POSTGRADUATE SCHOOL
PHYSICS & CHEMISTRY DEPT.
MONTEREY, CA 93943-5000

LIBRARY
NAVAL POSTGRADUATE SCHOOL
MONTEREY, CA 93943-5002

COMMANDER (2)
NAVAIRSYSCOM
ATTN: LIBRARY (AIR-723D)
WASHINGTON, DC 20361-0001

COMMANDER
NAVAIRSYSCOM, CODE 526W
WASHINGTON, DC 20361-0001

COMSPAWARSYSCOM
ATTN: CAPT. R. PLANTE
CODE 3213, NAVY DEPT.
WASHINGTON, DC 20363-5100

COMSPAWARSYSCOM
ATTN: CODE PWM 141
NAVY DEPT, BLDG NC1, ROOM 2E18
WASHINGTON, DC 20363-5100

COMMANDER
NAVAIRDEVCEN (3011)
ATTN: P. MOSIER
WARMINSTER, PA 18974

COMMANDER
NAVOCEANSYSCEN
DR. J. RICHTER, CODE 54
SAN DIEGO, CA 92152-5000

COMMANDER
NAVAL SURFACE WEAPONS CENTER
DAHLGREN, VA 22448-5000

COMMANDER
NAVSURFWEACEN, CODE R42
DR. B. KATZ, WHITE OAKS LAB
SILVER SPRING, MD 20903-5000

DIRECTOR
NAVSURFWEACEN, WHITE OAKS
NAVY SCIENCE ASSIST. PROGRAM
SILVER SPRING, MD 20903-5000

COMMANDER
NAVAL WEAPONS CENTER
DR. A. SHLANTA, CODE 3331
CHINA LAKE, CA 93555-6001

COMMANDER
NAVAL AIR TEST CENTER
PATUXENT RIVER, MD 20670

COMMANDER
PACMISTESTCEN
GEOPHYSICS OFFICER
PT. MUGU, CA 93042

COMMANDER
AWS/DNXS
SCOTT AFB, IL 62225

USAFETAC/TS
SCOTT AFB, IL 62225

AFGL/LY
HANSCOM AFB, MA 01731

COMMANDER & DIRECTOR
ATTN: D. R. BROWN
U.S. ARMY ATMOS. SCI. LAB
WHITE SANDS MISSILE RANGE,
NEW MEXICO 88002

DIRECTOR (12)
DEFENSE TECH. INFORMATION
CENTER, CAMERON STATION
ALEXANDRIA, VA 22314

DIRECTOR, ENV. & LIFE SCI.
OFFICE OF UNDERSECRETARY OF
DEFENSE FOR RSCH & ENG E&LS
RM. 3D129, THE PENTAGON
WASHINGTON, DC 20505

DIRECTOR, TECH. INFORMATION
DEFENSE ADV. RSCH PROJECTS
1400 WILSON BLVD.
ARLINGTON, VA 22209

WAVE PROPAGATION LAB
NOAA, ERL
325 S. BROADWAY
BOULDER, CO 80303

LIBRARY ACQUISITIONS
NCAR, P.O BOX 3000
BOULDER, CO 80307

LABORATORY FOR ATMOS. SCI.
NASA GODDARD SPACE FLIGHT CEN.
GREENBELT, MD 20771

DR. J.J. LIEBE
DOC/NTIA, INSTITUTE FOR
TELECOMMUNICATION SCIENCES
325 BROADWAY
BOULDER, CO 80303